BJR

https://doi.org/10.1259/bjr.20170508

Received: 10 July 2017 | Revised: 25 October 2017 | Accepted: 16 November 2017

Cite this article as:
Zaidi H, Karakatsanis N. Towards enhanced PET quantification in clinical oncology. *Br J Radiol* 2018; **90**: 20170508.

## REVIEW ARTICLE

# Towards enhanced PET quantification in clinical oncology

[1,2,3,4]HABIB ZAIDI, PhD, PD and [5,6]NICOLAS KARAKATSANIS, PhD

[1]Division of Nuclear Medicine and Molecular Imaging, Geneva University Hospital, Geneva, Switzerland
[2]Department of Nuclear Medicine and Molecular Imaging, University of Groningen, Groningen, Netherlands
[3]Geneva Neuroscience Centre, University of Geneva, Geneva, Switzerland
[4]Department of Nuclear Medicine, Universityof Southern Denmark, Odense, Denmark
[5]Division of Radiopharmaceutical Sciences, Department of Radiology, Weill Cornell Medical College of Cornell Univercity, New york, NY, USA
[6]Department of Radiology, Translational and Molecular Imaging Institute, ICAHN School of Medicine at Mount Sinai, New york, NY, USA

Address correspondence to:
Prof Habib Zaidi
E-mail: *habib.zaidi@hcuge.ch*
Nicolas Karakatsanis
E-mail: *nak2032@med.cornell.edu*

### ABSTRACT

Positron emission tomography (PET) has, since its inception, established itself as the imaging modality of choice for the *in vivo* quantitative assessment of molecular targets in a wide range of biochemical processes underlying tumour physiology. PET image quantification enables to ascertain a direct link between the time-varying activity concentration in organs/tissues and the fundamental parameters portraying the biological processes at the cellular level being assessed. However, the quantitative potential of PET may be affected by a number of factors related to physical effects, hardware and software system specifications, tracer kinetics, motion, scan protocol design and limitations in current image-derived PET metrics. Given the relatively large number of PET metrics reported in the literature, the selection of the best metric for fulfilling a specific task in a particular application is still a matter of debate. Quantitative PET has advanced elegantly during the last two decades and is now reaching the maturity required for clinical exploitation, particularly in oncology where it has the capability to open many avenues for clinical diagnosis, assessment of response to treatment and therapy planning. Therefore, the preservation and further enhancement of the quantitative features of PET imaging is crucial to ensure that the full clinical value of PET imaging modality is utilized in clinical oncology. Recent advancements in PET technology and methodology have paved the way for faster PET acquisitions of enhanced sensitivity to support the clinical translation of highly quantitative four-dimensional (4D) parametric imaging methods in clinical oncology. In this report, we provide an overview of recent advances and future trends in quantitative PET imaging in the context of clinical oncology. The pros/cons of the various image-derived PET metrics will be discussed and the promise of novel methodologies will be highlighted.

## INTRODUCTION

Image-guided diagnosis and treatment response monitoring in clinical oncology has benefited significantly over the last decades from the advent of quantitative molecular imaging techniques. Among those, positron emission tomography (PET) gradually emerged as the standard-of-care molecular imaging modality in clinical oncology owing to its relatively high sensitivity and specificity for a wide spectrum of oncological malignancies across the whole human body.[1] PET imaging relies on the positron/electron annihilation process to quantify the *in vivo* three-dimensional (3D) spatial distribution of a positron-emitting radiotracer associated with a specific molecular process. The resulting 3D PET images may elucidate the biochemical and functional state of specific biological mechanisms targeted by the employed radiotracer, as expressed in normal and cancer tissues, thus facilitating clinical diagnosis and staging evaluations as well as the monitoring of tumour metabolic response to therapeutic schemes over time.

The high sensitivity of PET is crucial for certain molecular imaging tasks involving very small, that is, trace amounts of the administered radiopharmaceutical, close to the minimum detectable activity concentration of a system.[2, 3] In addition, it may allow for adequate temporal sampling by dynamic PET of the rapid physiological changes in tracer

concentration, the latter induced by the specific pharmacokinetic attributes of the tracer in normal and tumour tissues.[4, 5] As PET images do not provide anatomical information, they are usually combined with co-registered anatomical data from other modalities, such as CT and MRI.[1, 6]

Furthermore, another powerful PET feature for clinical oncology is a high specificity, thanks to its capability of imaging specific molecular disease mechanisms, including, but not limited to, a broad range of oncological malignancies, each targeted by a specific positron-emitting tracer.[7] Moreover, multiple PET tracers could be administered to the same patient population to evaluate any potential associations between different pathological mechanisms, such as the processes of inflammation, proliferation, hypoxia and calcification, underlying the same or related types of malignancy.[8, 9] Furthermore, different PET tracers targeting complementary mechanisms of the same disease could be administered in the same scan session to allow for their co-registered evaluation before and during treatment.[10]

Nonetheless, the combination of high specificity and sensitivity may be only one of the factors for the widespread adoption of PET in clinical oncology. The other important feature is PET's unique highly quantitative signal, thanks to its inherent capability of measuring individual counts that can be related to the actual quantity of the underlying source distribution.[11, 12] The quantitative character of PET permits a clinically acceptable level of accuracy and reproducibility for a range of image-derived numerical metrics, such as the standardized uptake value (SUV) or the tracer macro- and micro-kinetic attributes, provided a sufficient amount of PET data is acquired and adequately corrected.[13, 14] Thus, PET imaging may enable the utilization of powerful numerical criteria to enhance reliability in diagnosis, prognosis and treatment response monitoring and facilitate theranostic PET-guided therapy protocols in clinical oncology.[11, 15]

However, a wide range of factors related to[16] the tracer interaction with the various physiological and pathological states of the different tissues, the physics principles regulating the production, emission and detection of the PET signal and finally the hardware and software features of modern PET scanners, may drastically affect the deterministic relationship between the actual tracer distribution and the estimated PET images. As such, PET quantification may be ultimately impacted if any of these effects is overlooked.[12, 17–21]

In this review, we highlight from a clinical perspective more recent efforts developed for the optimization of PET imaging protocols by focusing on novel methodologies aiming at improving PET quantification in the clinic. In particular, we discuss the impact of a classified set of acquisition and imaging factors on the quantitative value of PET and its relevance in clinical oncology. Furthermore, the latest methodological and technological developments designed to facilitate the adoption of dynamic 4D PET in the clinic for superior quantitative tumour analysis are briefly outlined. In addition, we describe a range of commonly used quantitative PET image metrics as well as their capabilities and limitations in quantitatively characterizing certain clinically relevant PET image features. A particular emphasis will be placed on the recent introduction of advanced four-dimensional (4D) whole-body (WB) PET imaging protocols,[22] thanks to the advent of highly sensitive time-of-flight (TOF) clinical PET systems[23] with improved resolution response modelling features within the image reconstruction process.[24] Finally, motivated by the current PET technology trends, we discuss the importance of combining conventional PET SUV analysis with dynamic WB PET acquisitions in order to translate the quantitative virtues of direct 4D PET image reconstruction and support truly multiparametric molecular imaging assessments in clinical oncology.

## Overview of physical and imaging factors impacting quantitative PET

The accuracy of PET measurements can be affected by (i) a range of physical effects related to the interaction of the emitted annihilation photons with matter and the detectors, as well as (ii) the PET system acquisition hardware and image reconstruction software performance.[25] Nonetheless, quantification may be more challenging in clinical practice where the scan time and the administered tracer dosage are strictly limited by radiation safety and patient throughput constraints, thereby denoting the importance of clinical PET scan protocol optimization.

A standard source of quantification errors in clinical PET studies is the overall attenuation of the emitted photons before detection.[26] The attenuation effects are caused by the physical interaction processes of photoelectric absorption and/or scattering away from the detectors of at least one of the two annihilation photons as they interact with matter intercepting their trajectory. As a result, a fractional loss of PET coincidence events occurs, which can be quantified with the energy- and tissue-dependent attenuation coefficient (AC) metric. The overall degree of attenuation of the emitted PET signal is expected to be more apparent in tissues of large volume and/or high AC values, resulting in significant, non-uniform loss of true PET counts and thus to artifacts and elevated statistical noise levels in the final PET images.[27]

Nevertheless, attenuation effects can be compensated by accounting within PET reconstruction for the 3D AC map, which can be directly measured from PET or CT transmission scans on hybrid PET/CT scanners.[28] In the absence of a transmission scan, as in the case of PET/MR systems, AC maps can be estimated indirectly from multi tissue-class or atlas-based segmentation of specific MR sequences.[29, 30] Furthermore, when TOF PET acquisitions of sufficient timing resolution are supported, AC maps may be directly reconstructed together with the respective emission maps from TOF PET data alone,[31] by employing simultaneous TOF reconstruction of emission and attenuation images. However, these methods estimate AC factors up to a constant offset,[31] thereby being susceptible to scaling issues or cross-talk between activity and attenuation images. In such case, regularized reconstruction algorithms may address these limitations by utilizing anatomical prior information from transmission or MR modalities.[32] In addition, when motion is present in the field-of-view (FOV), significant errors may be triggered during PET image reconstruction due to the potential

Figure 1. (Top) The principle of TOF PET acquisition and the distribution of counts to TOF bins along an LOR according to the time difference of the two annihilation photons' detection. (Bottom) Graphical illustration of the resolution degradation effects of (Top) positron range, (bottom) inter-crystal scatter and penetration, due to coincidences positioning in erroneous LORs. LOR, line of response; PET, positron emission tomography; TOF, time-of-flight.

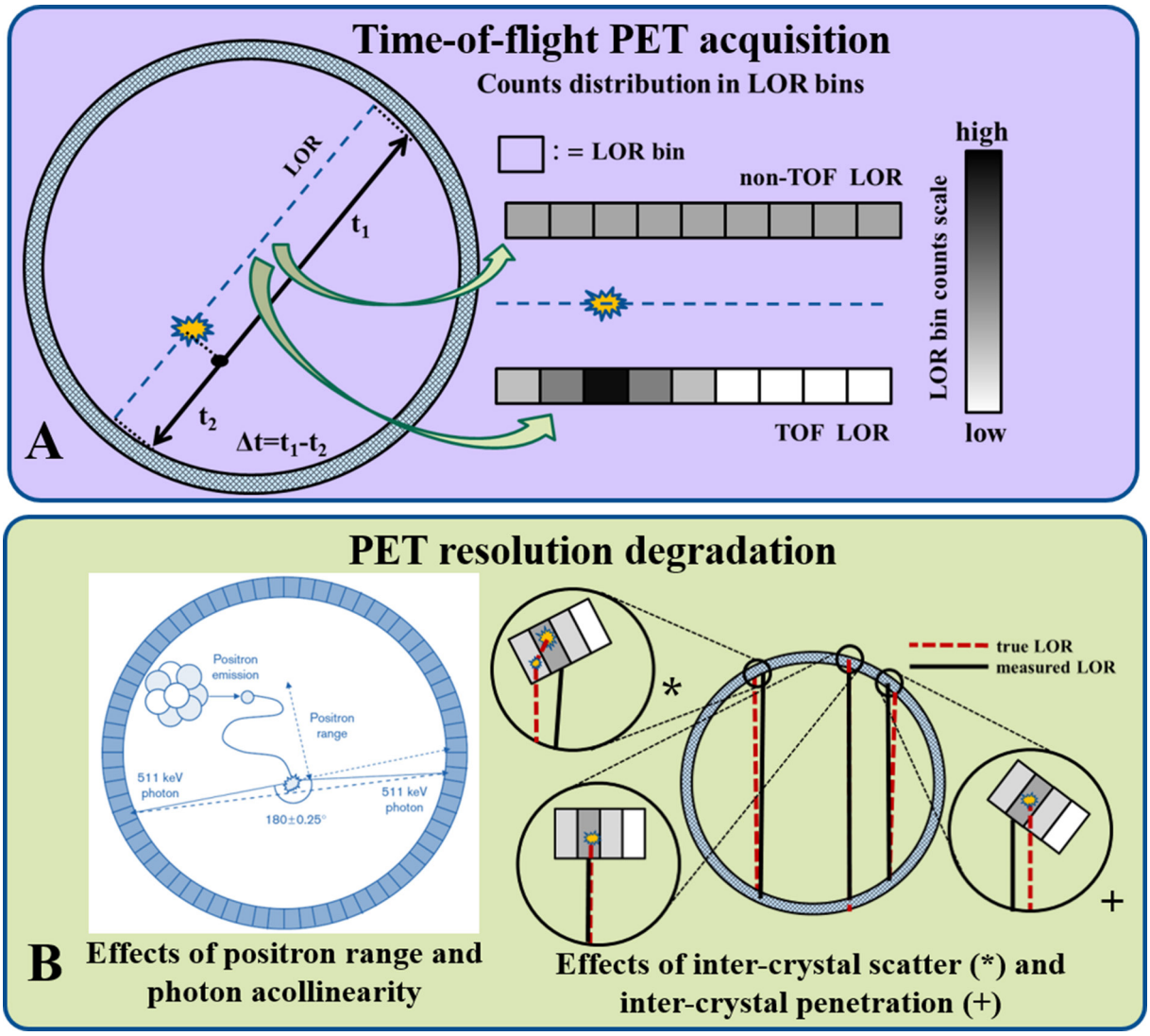


misalignment between the PET emission and attenuation data when the latter are estimated in breath-hold mode. The acquisition of free-breathing attenuation data could provide a rough first-hand solution in limiting the respiratory-induced attenuation-emission mismatches.[33, 34] Nevertheless, a more complete solution would be the motion correction of the attenuation and emission data.

Another class of errors in PET is triggered from the erroneous binning of coincidences to incorrect pairs of detectors or equivalently to lines of response (LORs) not intercepting the true annihilation position. The positioning of events to erroneous LORs may be triggered due to a variety of PET resolution degradation factors, such as random or scatter events, positron range, annihilation photons acollinearity, inter-crystal penetration or motion (Figure 1).

Random or accidental coincidences may occur when two photons from different but nearly simultaneous annihilations are detected accidentally as a single coincidence event. Their likelihood increases proportionally to the square of the tracer activity in the FOV. Scatter coincidences occur when the straight trajectory of at least one of the two annihilation photons is deflected while travelling through the imaging subject body (body scatter) or a detector element in its path (inter-crystal scatter). As a result, photons lose part of their kinetic energy and are deflected such that they either i) escape detection, thus leading to the loss of the coincidence event (attenuation), or ii) stop at a detector not located along their original LOR line path, thereby triggering a scatter coincidence assigned to an erroneous LOR position.[35] Moreover, scattering of photons emitted from annihilation points outside the FOV may also generate scatter counts.[36] Scatter events are associated with significantly smaller amounts of

energy deposited to the crystal point of interaction. Thus, scatter effects can be limited by simply rejecting coincidence events with deposited energies outside the expected energy window for true coincidences, given the energy resolution of the PET system. However, model-based scatter correction using patient-specific attenuation maps and mathematical scatter models proved to be a more accurate approach compared to conventional energy-based techniques and is the de facto standard scatter correction method implemented by current scanner manufacturers.[35]

Positron range refers to the distance travelled by an emitted positron before losing all its kinetic energy and being annihilated with an electron. As a result, the annihilation points are forming a uniform distribution around the actual emission point, thereby causing image blurring for positron ranges larger than the system's intrinsic spatial resolution.[37] Nonetheless, in the case of integrated PET/MR, the presence of a strong magnetic field may limit positron range along certain directions due to magnetic forces exercised on positron's trajectory.[38] Moreover, annihilation photon acollinearity effect describes the cases where the two annihilation photons are emitted apart at an angle with respect to one another other than 180 degrees. As a result, the two photons may be detected at two opposing detectors whose LOR does not intercept the true annihilation position. Thus, for a given emission angle other than 180 degrees, the acollinearity effect is expected to trigger a resolution loss or blurring proportional to the average distance the photons travel before hitting a detector, the latter being directly proportional to the scanner detector ring diameter.[39]

Inter-crystal penetration involves the undetected crossing of a photon through the first crystal detector intercepting its path, before its final detection in another proximal detector. This effect mainly occurs for photons scattered within the first crystal or photons hitting the front surface of the first crystal at a relatively large angle of incidence, such that its trajectory path length within that crystal is not sufficiently long for its complete stop before penetrating to the next crystal intercepting the photon path. In both cases, the photon is eventually detected in a different detector from the one it first intercepted, thereby resulting in an erroneous LOR assignment, .[40] In the first case, the error is related to the inter-crystal scatter effect previously outlined. In the second case, the error is associated with the angle of incidence and may be compensated by accounting for the actual depth at which the photon was absorbed within the crystal. Th is metric, also known as depth-of-interaction (DOI), is defined by the distance of the point of absorption from the crystal front surface and can be approximated by employing multiple layers of different detectors parallel to the front surface .[41] The DOI effect is more apparent for large incident angles as expected either for smaller detector ring diameters, for photons originating from the edges of the transaxial FOV or for photons travelling along very oblique LORs.

Partial volume effect (PVE) is another important source of PET quantification bias that has been recognized as an important image resolution and quantification degradation factor, especially for small lesions. Owing to the limited spatial resolution of clinical PET systems, the PET signal at high activity regions is expected to spill over any neighbouring low activity regions. As a result, small hot lesions may appear blurred and larger in volume but with an underestimated average activity concentration. Equivalently, the tracer activity in cold lesions may be overestimated due to spill-in of signal from the surrounding higher activity regions. Consequently, the detectability of both hot and cold lesions may be affected. A number of strategies have been devised to address the PVE problem in the context of molecular PET imaging by operating either on the reconstructed images or within the reconstruction process with many of them relying on adjunct coregistered anatomical images (CT or MRI).[42, 43]

Finally, motion during PET acquisition may cause LORs translation and attenuation-emission mismatches, thereby resulting in non-negligible resolution degradation and quantification bias.[44] The effects of motion can be estimated and later modelled in the system resolution response matrix for correction during reconstruction either in the list-mode data space by translating each event's LOR to the correct position or, in the image space by applying a 3D motion transformation.[45] However, event-by-event PET motion correction is considered the gold standard approach, as it inherently accounts for the difference in PET system sensitivity and normalization correction factors between the original and translated LORs of each detected event, particularly when one of the two LOR positions involves a detector gap or a point outside the FOV.[46]

Nowadays, virtually all state-of-the-art clinical PET systems are equipped with TOF acquisition technology, which can approximate the position of each detected event along a small LOR segment, known as TOF bin, based on the difference between the two annihilation photons detection time, thanks to the superior timing resolution of modern detectors. TOF PET reconstruction methods have currently demonstrated significantly increased robustness to data inconsistencies, such as attenuation-emission mismatches or AC inaccuracies, owing to their inherent feature of limiting the associated errors propagation within the small LORs segments from which they originate, rather than the entire LORs.[47, 48]

Moreover, image-based iterative deconvolution or deblurring methods have been recently applied, after or within the PET reconstruction process, as a practical and clinically adoptable approach to effectively recover losses in PET image quantification and contrast due to various resolution degradation factors, such as point spread function (PSF) and motion effects.[49, 50] These methods commonly employ image blurring kernel functions estimated from a series of experimental measurements, simulations or analytical calculations to model a particular resolution degradation effect.

A first example of deconvolution methods within PET image reconstruction is PSF reconstruction algorithms, also known as resolution or partial volume recovery reconstruction methods.[24] In particular, image PSF kernel functions can be constructed from measured, simulated or calculated PSF PET data to model the space variant overall blurring effect due to a series of spatial

resolution degradation factors, such as positron range, scattering in the detectors, inter-crystal penetration and photons acollinearity. The measured PSF resolution kernel may be modelled within the PET image reconstruction framework by nesting a Richardson-Lucy iterative image PSF deconvolution process within each global tomographic image update step to effectively accelerate the overall convergence of the algorithm.[49, 50] Moreover, recent studies explored PSF kernels of slightly different sizes than those actually measured, as a way to perform task-based tumour quantification and reduce ring or edge Gibbs artefacts, commonly observed in deblurred images after a large number of deconvolution iterations.[24]

Similarly, the total motion tracked within a PET acquisition frame can be efficiently modelled as a kernel blurring image function, which can later be deconvolved via an analogous nested iterative deconvolution method. Unlike standard 4D motion-compensated image reconstruction algorithms requiring multiple gates of PET data and periodic motions,[51] the motion deconvolution process may be conveniently nested within a simpler 3D reconstruction algorithm of standard ungated PET data to enhance clinical adoption.

## WHY DO WE NEED QUANTITATIVE IMAGING IN CLINICAL ONCOLOGY?

PET has historically been interpreted qualitatively by qualified physicians trained to pinpoint metabolic abnormalities and distinguish them from a normal biodistribution and from typical pitfalls associated with this imaging modality. Qualitative visual interpretation is still the de facto standard technique used in most clinical facilities worldwide. However, this approach suffers from inter- and intra-observer variability owing to its subjective nature.[17] In the meantime, clinical PET guidelines have recommended the usage of semi-quantitative metrics requiring various assumptions. Although simple and practical for use in the clinic, semi-quantitative metrics are subject to a number of approximations implicit in the use of uptake ratios that may also lead to variability and bias.[52] As such, their use for robust disease monitoring and assessment of treatment response as well as in clinical trials requires standardization of PET quantification techniques to enable pooling data across different facilities or scanners using different data acquisition and reconstruction protocols.[53, 54]

The Quantitative Imaging Biomarkers Alliance® (QIBA®) initiated by the Radiological Society of North America (RSNA) defined quantitative medical imaging as *"the extraction of quantifiable features from medical images for the assessment of disease, injury, or chronic condition relative to normal"* (rsna.org/QIBA). Therefore, quantitative imaging covers the whole chain encompassing the development, standardization and optimization of multimodality (anatomical, functional and molecular) image acquisition protocols, image analysis and visualization techniques, as well as structured reporting of results and findings. The wide clinical adoption of hybrid PET/CT utilizing TOF and PSF reconstruction technology along with the enthusiastic deployment of novel simultaneous PET/MRI in a significant number of academic institutions were among the technical advances that further motivated the interest in quantitative PET in clinical oncology.

Figure 2. Overview of image-derived PET metrics currently used in clinical and research applications in clinical oncology. PET, positron emission tomography.

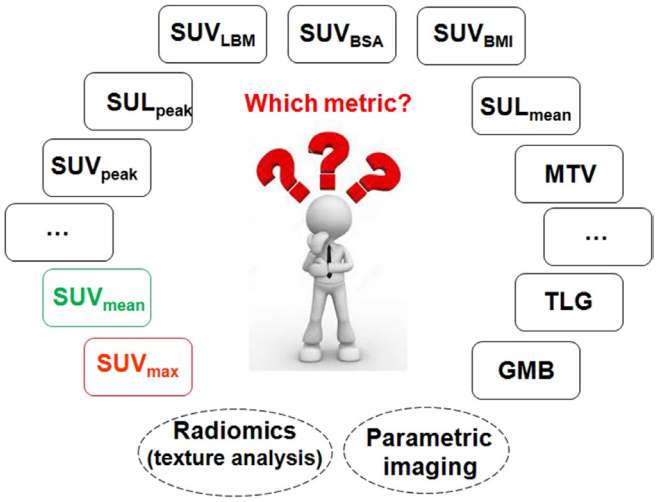


However, quantitative PET imaging is still hampered by a number of physical, technical and physiological factors widely discussed in the scientific literature.[16] All scanner manufacturers devised appropriate techniques and end-user software to compensate for common physical degrading factors, such as attenuation of annihilation photons and Compton scattering. However, more intricate issues, such as motion and partial-volume-averaging are not yet addressed on commercial systems. Therefore, there is an urgent need for incorporation of motion and PVE correction features in commercial packages to enable full integration of quantitative molecular imaging in the clinic. In addition, the large variability of study performance across institutions and the lack of consensus on the metric that should be used in clinical oncology delayed the integration of PET as a quantitative imaging biomarker into phase I-III clinical trials.[15] Indeed, it is intriguing to review in perspective the considerably large number of metrics reported in the scientific literature, which makes life of novice end users difficult (Figure 2). It is anticipated that the deployment of advanced quantitative PET imaging techniques in the clinic will expand as novel specific tracers are embraced in diverse clinical applications.[19]

### Static whole-body PET imaging

Static WB PET imaging involves the temporal integration of all acquired coincidence events (counts) within a particular scan time period in a single time frame of data at each bed position. Initially, the time-ordered list of detected counts acquired within a time frame are histogrammed to their respective LOR positions or bins to ultimately form a 3D sinogram for that time frame. Later, the produced sinogram is reconstructed to estimate the 3D spatial distribution of the estimated PET tracer activity concentration over the frame. Alternatively, the activity concentration can be directly estimated from the temporal stream of PET coincident events on an event-by-event basis via a list-mode

reconstruction algorithm. In both list-mode and sinogram-based 3D reconstruction methods, a single static PET image is created at each bed position and time frame, depicting the 3D spatial distribution of the tracer activity concentration, in units of Bq $ml^{-1}$, over the respective time frame.

To improve standardization of the static PET images and enable their quantitative comparison, the activity concentration values at each voxel are first corrected for decay and then normalized with the ratio of the body mass over the administered amount of radiotracer dosage. The resulting SUV metric has been currently established in nuclear medicine .[13] Depending on the volumetric properties and location of each targeted region of interest (ROI) of a study, the mean, maximum or peak SUV value may be calculated. In addition, the target-to-background ratio (TBR) and the contrast-to-noise ratio (CNR) scores may also be evaluated between target and background ROIs drawn on static PET images. Nonetheless, the tracer spatial distribution in living tissues changes dynamically with post-injection time, as regulated by its *in vivo* physiological uptake properties. As a result, PET images estimated from 3D static reconstruction methods may only represent the average 3D distribution of the tracer over a single time frame. Thus, the larger the time frame or the faster the tracer kinetics at that frame is, the less representative the static PET image is expected to be of the tracer distribution at any given moment of the acquisition. Thus, the time frame position, relative to injection time, should be chosen such that the activity concentration in most regions of interest remains relatively stable throughout the selected frame, to avoid significant temporal variance of the counts before their integration for improved quantitative accuracy. In addition, the bed frames post-injection time position should be selected, such that sufficient activity uptake and contrast is achieved in the target relative to the respective background ROIs, with enough temporal stability to ensure satisfactory noise-equivalent count statistics and minimum temporal count variance.

Therefore, the following three parameters should be considered when optimizing static PET imaging protocols for each new tracer and scanner system combination: the radiotracer decay rate, the nominal sensitivity of the employed PET scanner and the tracer kinetics. For the latter, dynamic PET imaging can be very useful, as it can estimate the frame post-injection time position for which the PET signal TBR in the target ROIs is maximized or becomes relatively stable for the employed tracer.

In the case of multibed static PET imaging protocols, the scan time window optimization can be conducted for every bed position.[55] In most clinical PET protocols, the scan duration is set constant across all bed positions such that the varying quantitative accuracy and precision is always maintained above clinically acceptable levels while the protocol retains its simplicity for clinical adoption. Nonetheless, in order to ensure sufficient quantification across all bed positions, the distribution of the total attenuation and emission signal should be accounted for each bed position. Then, a certain subset of beds may be favoured over others in terms of scan time, particularly if the expected ROI signal contrast is too low for these bed positions due to tracer low uptake kinetics in the ROIs or highly attenuating proximal tissue.[55]

Moreover, multibed or WB PET acquisitions have initially been conducted in the clinic across successive stationary bed axial positions after step-wise translation of the scanner table from one position to the next. This WB PET scan mode, known as step-and-shoot (SS) acquisition, has been currently established in all multibed or WB PET clinical protocols, thanks to the convenience of binning the counts to stationary LOR bin positions. Meanwhile, fully 3D PET acquisitions were introduced in the clinic for enhanced sensitivity and count rates.[56] Unlike two-dimensional scans, the sensitivity gain in 3D PET acquisitions is significantly higher in the central section of the PET axial FOV due to the enhanced coverage of this FOV section by the additional oblique LORs involved in fully 3D PET scans. As a result, 3D PET scans at each bed position are characterized by a significantly imbalanced axial sensitivity profile where considerably higher statistical noise levels can be observed over the two axial edges of each bed position compared to its centre.

Multibed PET SS protocols require a significant overlap between successive bed positions effectively doubling the scan time in the overlapped bed edges to compensate for their lower sensitivity.[56] As a result, the stationary bed acquisitions involved in SS mode force the independent reconstruction of the relatively fewer counts at each bed edge followed by their summation/overlapping in the image space. As the overlapping is conducted at the image level, rather than the projection data space, relatively high statistical noise levels are expected in the overlap regions compared to the rest of the PET FOV. Naturally, the noise amplification in the overlapped sections with respect to the axial centre of the PET images becomes more significant for multibed imaging protocols, especially when involving short individual bed scan times, as then very low counts are expected per bed position for a given scanner sensitivity. Consequently, quantification of tumours or other lesions located in the overlapped regions may be considerably degraded in multibed SS PET. In addition, modern clinical PET scanners currently overlap more than half of their axial FOV in total, thereby leaving only a small central axial FOV fraction outside the overlap regions. Consequently, there exists a significant probability for quantitative errors due to non-uniform axial sensitivity in multibed PET SS imaging.

Nevertheless, an alternative multibed scan mode involving a smooth continuous bed motion (CBM) during PET acquisition may address the previous limitation of multibed PET scans.[57] In the case of constant bed speeds, each transaxial slice of the subject body will be scanned in all axial positions of the scanner FOV for the same amount of time as the bed moves. Thus, unlike SS mode, the axial sensitivity profile in CBM mode is expected to be uniform across all transaxial slices of a scanned body, except at the start and end position of the moving bed. In Figure 3, we present the expected axial sensitivity profiles of SS and CBM PET acquisition modes along an axial FOV corresponding to a total of three conventional bed positions. Furthermore, CBM also retains the ability to apply customized bed speed axial profiles to compensate for any significant total counts variance expected

Figure 3. Axial 3D PET sensitivity profile along a FOV covered by three bed positions of a modern clinical PET scanner system for (top) SS and (bottom) CBM acquisition modes. CBM, continous bed motion; FOV, field of view; PET, positron emission tomography; SS, step-and shoot.

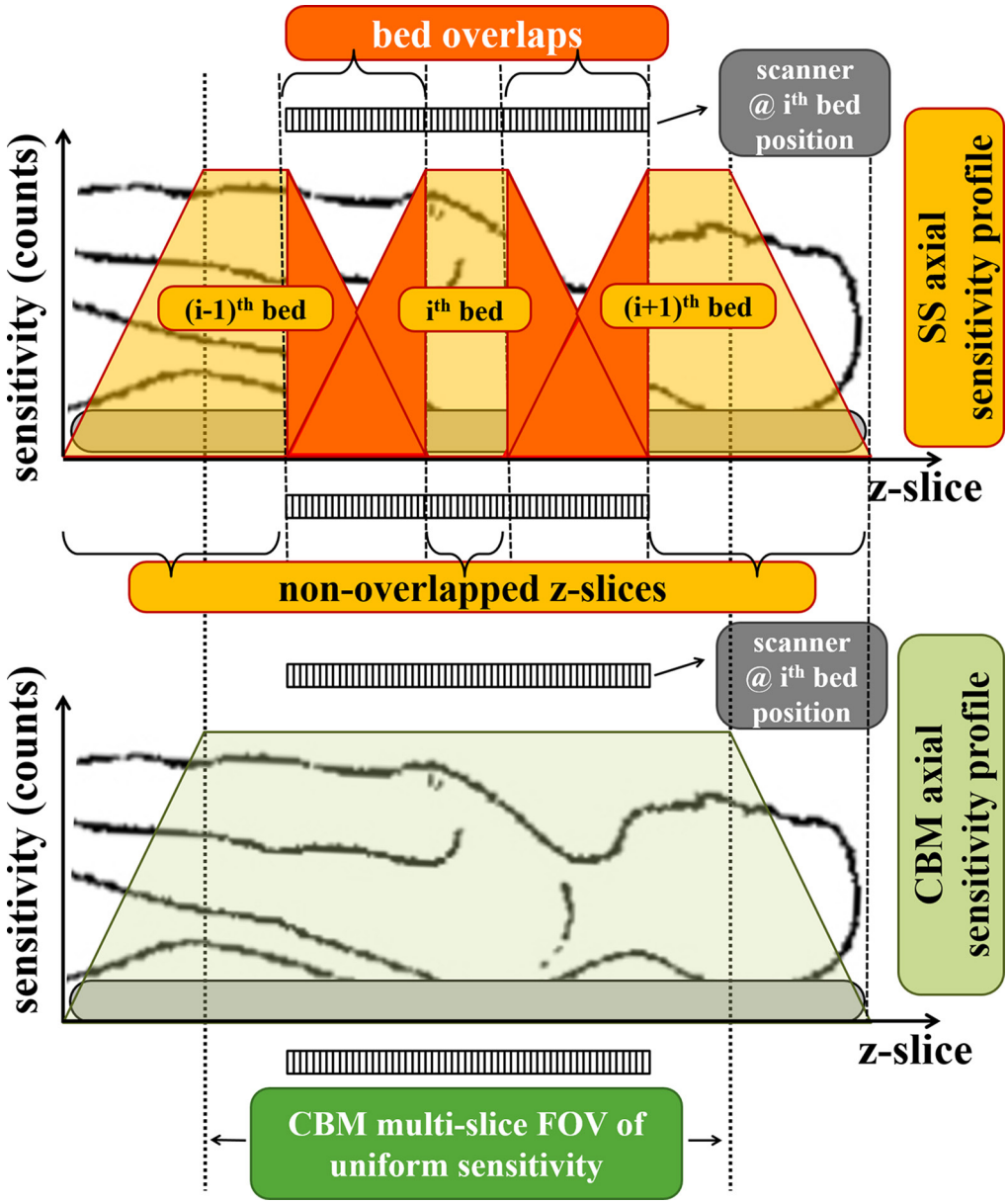


along the axial direction, based on the variable degree of attenuation and the local intensity of the tracer activity concentration. Thus, CBM PET imaging protocols can be further optimized to attain uniform statistical noise distributions across the entire axial FOV for enhanced quantification of potential metastatic tumour lesions in clinical oncology PET studies.

However, in CBM mode, each transaxial slice of the scanned body is sampled for a unique scan time window, whose position is shifted compared to that of successive slices. Thus, a different average time stamp should be assigned to the CBM data of each transaxial slice, as opposed to each bed for SS data, thereby introducing different decay correction factors and temporal tagging per slice for the valid dynamic and parametric analysis of WB 4D PET CBM data.[58] Moreover, the CBM mode allows for binning and subsequent reconstruction of the PET data from any continuous set of slices of the total axial FOV, without being limited to fixed bed positions as in the case of SS mode.[57] Essentially, CBM technology permits the setting of the total axial FOV in terms of number of slices, rather than in terms of number of beds, thereby allowing the utilization of the minimum necessary axial FOV needed for a particular PET study to minimize total PET scan time, especially in WB dynamic PET acquisitions involving multiple WB passes, or to minimize CT dose in PET/CT studies. As an analogy to SS multibed scans, CBM acquisitions extending axially beyond a single bed FOV could be referred to as multislice scans. The multislice PET data are later grouped into groups or "chunks" of slices, each consisting of the same number of slices

as the beds in SSmode. The term "chunk" is used to differentiate these slice groups of CBM mode from the "beds" or "bed positions" of SS mode, as the former are not associated with a fixed axial position. Then, all LOR counts belonging to the 3D space defined by the respective chunks are histogrammed to build the respective chunk sinograms, that are subsequently reconstructed using the same system matrix as for the conventional SS PET sinogram reconstruction. The chunks are overlapped to the same axial extent as the successive beds of SS acquisitions to ensure all acquired CBM data at the chunk edges are sorted into the respective chunk sinograms. Thus, a uniform axial sensitivity profile is retained along all chunks, except of one of the edges of the first and last chunk. The PET reconstructions from multiple axial slice chunks of CBM data could be referred to as multichunk CBM PET reconstructions.

## LIMITATIONS OF STATIC IMAGING AND CHALLENGES OF DYNAMIC IMAGING

Static PET imaging involves by definition a single time point acquisition over a particular scan time window. However, the measured activity concentration signal follows a dynamic trend in the various organs and tissues, as dictated by the tracer pharmacokinetic properties under normal and pathological conditions.[4, 5] Consequently, static PET imaging may only provide a "snapshot" of the administered tracer distribution averaged over a particular static frame, thus considerably limiting the amount of unique *in-vivo* molecular information needed for more accurate diagnostic, prognostic and treatment response assessments.

Despite correcting for decay and normalizing activity concentration with respect to the administered tracer dosage and subject (lean) body mass, the well-established SUV clinical metric may still depend to a great extent on the post-injection time, and the time course of the PET activity concentration in the blood plasma(input function). The effect of these factors on SUV may pose considerable quantitative limitations for the objective comparison of PET images across different scans, such as in the case of treatment response monitoring.[59] Consequently, in view of these limitations, SUV can be considered a semi-quantitative surrogate index of tumour metabolism.

On the other hand, dynamic PET involves the spatiotemporal acquisition of PET data in tissues of interest as well as in the blood plasma. The acquired 4D PET data may subsequently be utilized by graphical analysis or compartmental kinetic modelling methods to enable imaging of highly quantitative physiologic parameters of the tracer dynamic activity distribution, beyond the SUV metric. The dynamic acquisition may either be limited to a single bed for continuous temporal sampling of the tracer activity concentration after injection or, extended over multiple beds by introducing fast multiple WB scan passes , as recently became feasible with the advent of higher sensitivity PET scanners and the introduction of clinically adoptable dynamic WB PET clinical protocols.[22, 60, 61] Moreover, the respective blood plasma input function can be derived either from (i) arterial blood samples, (ii) dynamic PET image ROIs drawn on heart ventricles, the aorta or other mediastinal blood pool regions, or (iii) population-based input function models.[62, 63] Subsequently, the complete 4D PET data of each bed and the derived input function can be fitted to an appropriate graphical analysis or compartmental model, provided the associated model assumptions regarding the tracer kinetic attributes in the targeted regions are satisfied, to estimate a specific set of physiologic tracer kinetic parameters. When the fitting is performed at the voxel level, a set of highly quantitative parametric PET images can be estimated.

The three major classes of dynamic PET analysis methods often employed in oncology studies are the fully compartmental kinetic models, which involve the least number of assumptions but also a large number of free microparameters,[4, 5] the graphical analysis methods[14, 22, 64, 65] employing linearized functions of kinetic macro-parameters and the single-scan auto-radiographic techniques that are usually the simplest but often the least accurate.[66] The latter methods require a very small number of dynamic PET frames at later post-injection times without an input function, thus are considered easily adoptable in the clinic. Nevertheless, they rely on quite restrictive kinetic assumptions or/and a-priori knowledge of certain kinetic parameters or input function features. As a result, they may be valid only for very specific tracers, tissues and protocols, which considerably restricts their application scope in clinical oncology.[66] Therefore, in this review we will only refer in detail to the first two method classes.

The compartmental methods involve the least number of theoretical assumptions and stem from the hypothesis that all administered tracer molecules are expected to be at any given time at one of the model compartment states.[67] Each compartment is defined as the tracer activity concentration at one of the various possible combinations of states, primarily in terms of physical location (*e.g.* extracellular or intracellular tissue) and chemical condition (*e.g.* metabolized or not). The free parameters in this model class are defined as the positive kinetic rate constants

Figure 4. (a) Block description of a 2-tissue 4-parameters compartmental kinetic model employed for the widely applicable $^{18}$F-FDG radiotracer in clinical oncology. (b) Mathematical definition of the tracer influx rate constant $K_i$ macro-parameter as a non-linear combination of the individual microparameters $K_1$, $k_2$, $k_3$ and $k_4$ (rate constants) of the $^{18}$F-FDG compartmental model. (c) Characteristic $^{18}$F-FDG tissue time activity concentration curves (TACs) as modelled with the full 2-tissue compartmental model and published $^{18}$F-FDG measured kinetic parameters. FDG, fludeoxyglucose; TACs, time activity concentration curves.

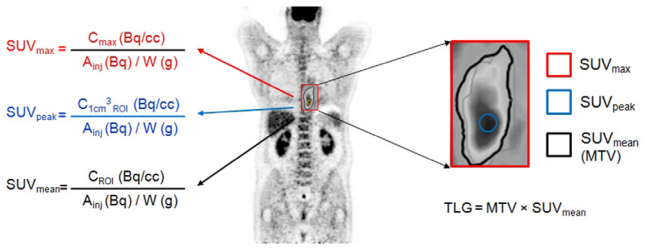

regulating the tracer molecules state transition between any pair of linked compartments (Figure 4).

In general, the number of compartments and kinetic rate constants are expected to increase with the level of detail employed to model the underlying biochemical mechanisms regulating the tracer's *in vivo* physiological uptake. In particular, the standard fully compartmental kinetic model currently employed for the $^{18}$Fluorodeoxyglucose ($^{18}$F-FDG) tracer, which is the most commonly applicable PET radiotracer in clinical oncology, is a 2-tissue compartment 4-parameter model describing the transition of $^{18}$F-FDG between blood and its exchangeable and metabolic tissue states (Figure 4).[4] The compartmental kinetic models are associated with large complexity and relatively high noise levels, due to the relatively high degree of their differential equations and the large set of free non-linear parameters involved. Therefore, a high number of dynamic frames per bed may be crucial to attain sufficient precision in the parameter estimates, especially for the first few minutes after injection, where input function and tissue uptake change rapidly with time. Moreover, in case of multibed and particularly WB FOVs, each bed should be sampled at a very high temporal rate, especially at early times where rapid tracer kinetics are involved, in order to attain sufficient temporal sampling across all beds. Consequently, fully compartmental modelling over WB FOVs is practically not feasible in the clinic and thus confined to single-bed FOVs.

On the other hand, the graphical analysis methods are designed for the direct estimation of a reduced set of macro-parameters, which nevertheless still contain the principal and clinically relevant components of the tracer kinetic properties. As an example, two widely applicable graphical analysis methods for the robust dynamic analysis of single-bed PET irreversible and reversible uptake data are the standard Patlak (sPatlak)[14] and the Logan plots,[64] respectively. The sPatlak method has been designed to primarily image the tracer net uptake or influx rate constant $K_i$ Figure 5, while Logan plot targets the distribution volume *DV* parameter, with both macro-parameters considered of high clinical interest in oncology. In effect, the tracer kinetic macro-parameters conveniently summarize most of the clinically useful kinetic information content of the compartment parameters,

Figure 5. Flowchart demonstrating a clinically adoptable dynamic WB $^{18}$F-FDG PET acquisition protocol performed at a standard-of-care acquisition window 60 min post $^{18}$F-FDG injection for potential combined production of both $K_i$ and noise-equivalent SUV WB PET images. The particular version consists of six WB passes, each consisting of six beds, each of 30 s acquisition, as optimized for the Siemens Biograph™ mCT TOF PET/CT system. FDG, fludeoxyglucose; PET, positron emission tomography; SUV, standardized uptake value; TOF, time-of-flight; WB, whole body.

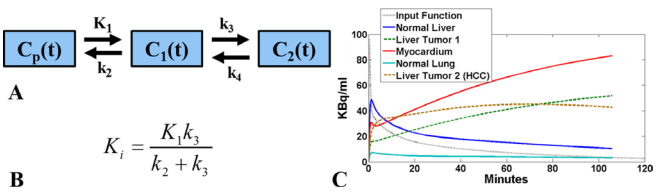


the latter also known as microparameters. The relative quantitative advantage of graphical analysis methods over compartmental models lies on their superior robustness to the high noise levels often expected in 4D PET data, especially when acquired across WB FOVs. Recently, a clinically adoptable dynamic WB $^{18}$F-FDG PET scan protocol was introduced involving an initial short dynamic acquisition over the heart, beginning at $^{18}$F-FDG injection time, followed by a series of fast WB passes (45sec/bed) to capture the $^{18}$F-FDG kinetics within the first 30-40min post injection (Figure 5). In order to image the Ki macro-parameter across the multiple beds of the acquisition, the sPatlak method was applied to the dynamic PET images and an input function, the latter derived from a region drawn at the heart left-ventricle across the dynamic PET images.[22, 68]

In addition, a useful generalization of the sPatlak model had also been proposed, namely the generalized Patlak (gPatlak) plot,[14] which has recently been adopted for WB $^{18}$F-FDG PET parametric imaging for enhanced quantification of Patlak $K_i$ images in the case of $^{18}$F-FDG uptake reversibility.[22, 65] In particular, gPatlak begins with the assumption of a small positive $k_4$ microparameter for the $^{18}$F-FDG 2-tissue compartment model to derive an extended non-linear Patlak plot that is capable of accounting for a potentially non-negligible but mildly positive reversibility in tracer uptake.[69] As a result, gPatlak method may enhance quantitative accuracy of $K_i$ parametric images in regions with non-negligible $^{18}$F-FDG uptake reversibility, where sPatlak would have underestimated $K_i$ by neglecting $k_4$.[65] Although gPatlak retains most of the robust features of the Patlak family offering high clinical adoptability, it is a non-linear method and thus may not be as robust to noise as the linear sPatlak method, unless applied in the context of direct 4D reconstruction as it has been recently demonstrated with clinical oncology PET data.[70 71]

Finally, a combination of the standard-of-care WB PET SUV imaging with the advanced Patlak $K_i$ imaging has been recently proposed for oncology studies by introducing a novel and clinically feasible dynamic WB $^{18}$F-FDG PET/CT protocol that utilizes the same exact scan time window previously employed for static SUV protocols.[72] In particular, the hybrid SUV/Patlak protocol is designed such that the total amount of WB dynamic (4D) PET data acquired over multiple WB fast scan passes is noise-equivalent to the data amount that would have been collected within the same scan time window if a single-pass WB 3D PET SUV-only protocol was applied. The dynamic WB PET data may, then, be summed over the multiple passes at each bed position to synthesize a static WB PET dataset, which can be later reconstructed to produce a noise-equivalent WB PET SUV image, as well as dynamically analysed to simultaneously estimate a WB $K_i$ image by fitting the multipass data to either the sPatlak or gPatlak model through indirect post-reconstruction analysis[72] or direct 4D reconstruction methods..[73]

Nevertheless, since the standard-of-care scan time window of conventional SUV-only $^{18}$F-FDG PET studies begins only 1 h after injection, the $^{18}$F-FDG PET data from the first 1 h after injection are not acquired with the SUV/Patlak protocol. Therefore, a

population-based input function model may be used to extrapolate from the late time window measurements the missing early section of the input function and thus enable calculation of the input function temporal integral for the Patlak analysis.[63]

The combined SUV/Patlak multipass imaging method could potentially replace in the future the conventional single-pass WB SUV-only clinical protocols without affecting the current throughput of a clinic. Such framework could thus enable the co-registered evaluation of WB SUV and $K_i$ images from a single standard-of-care WB scan session to potentially enhance the quantitative value of diagnostic and theranostic PET exams in modern clinical oncology.

## IMAGE-DERIVED PET METRICS

A number of PET metrics have been devised and used in clinical and research settings. These range from simple semi-quantitative metrics, such as the SUV to high order metrics that require advanced image analysis techniques.[74] The last category of techniques, more suited for research applications where there is greater emphasis on quantitative accuracy, requires dynamic acquisition protocols and advanced mathematical models to support rigorous kinetic analysis for absolute quantification of the PET data. According to the classification adopted in the reference above, four different categories can be defined and are discussed below.

### First-order metrics: $SUV_{max}$ and $SUV_{peak}$

The SUV metric has been adopted in clinical oncology as a semi-quantitative quantity indicating the amount of FDG uptake in a malignant lesion at a defined time post-injection, The uptake is normalized to the ratio of the injected activity dosage over the patient's weight, which represents the tracer whole-body distribution volume.[13] The SUV concept is very popular and used in a large number of centres owing to its simplicity and practicality since only a WB static image is required compared to cumbersome fully quantitative protocols using kinetic modelling, which require dynamic studies and continuous arterial blood sampling. SUV calculations are commonly implemented on commercial and non-commercial image display and analysis platforms. Caution is needed since substantial variability was reported among the different platforms and software packages available today.[75] Regardless of the platform and whether it is commercial or non-commercial, most software packages calculate SUVs normalized to patient's body weight. However, other variants where the SUV is normalized to other quantities have also been suggested to take into account the fact that adipose tissue is not as metabolically active as other tissues. This includes normalization to lean body mass ($SUV_{LBM}$ or SUL)[76] and body surface area ($SUV_{BSA}$),[77] which were both thought to be more relevant than the standard practice of using body weight for characterization of metabolically active abnormalities and less susceptible to variance attributable to body habitus.[19] SUL was reported to be less prone to variability and stable among patients in contrast to SUV normalized to body weight.[15]

The most commonly used metrics in the clinic are the mean and maximum SUV ($SUV_{mean}$ and $SUV_{max}$). The former represents the average SUV in all pixels or voxels in a defined ROI or volume of interest (VOI), whereas the latter represents the highest SUV score in the same ROI or VOI (Figure 6). For the specific task of PET-based monitoring of response to treatment, $SUV_{max}$ is known to be very sensitive to noise, since its definition relies on a single voxel within the whole volume. On the other hand, $SUV_{max}$ is less sensitive, compared to $SUV_{mean}$, to the tumour contour delineation method employed to extract the set of image voxels based on which these metrics will be calculated. In addition, $SUV_{peak}$ has been promoted as a more robust metric of less susceptibility not only to tumour delineation but also to noise artefacts. It is calculated as the mean SUV in a spherical VOI of 1.2 cm diameter (volume of 1 ml) centred at the most active portion of the tumour (Figure 6).[15] There is an assortment of definitions of $SUV_{peak}$ depending on the delineated VOI, which can substantially impact the end result.[78] Because of the relatively smaller sensitivity of $SUV_{max}$ and $SUV_{peak}$ to the tumour delineation techniques, they are considered in this review as first-order static image metrics.

### Second-order metrics: $SUV_{mean}$, TLG and MTV

Unlike $SUV_{max}$ and $SUV_{peak}$, mean SUV ($SUV_{mean}$) can be very sensitive to the technique used in delineating the lesion contour and, as such, is more prone to PVE-induced errors.[42] This delineation, which segments the voxels of a PET image into two distinct classes, namely the tumour and normal tissue, may also determine the definition of the metabolic active volume (MTV). This process is commonly performed manually as the de facto standard used in clinical centres. The total lesion glycolysis (TLG) is then calculated by multiplying $SUV_{mean}$ by the MTV.[79] The conceptual basis of the TLG is to provide a quantity linked to the global metabolic response of the whole lesion, which complements the SUV metric and its variants. The TLG is reproducible and was reported to be highly correlated with other PET metrics used in the assessment of response to treatment.[19] The $SUV_{mean}$, MTV and TLG metrics are considered second-order static PET image metrics as they are highly dependent on the technique and assumptions employed to delineate a tumour contour.

PET image segmentation plays a critical role for characterization of metabolic abnormalities, assessment of response to treatment and definition of treatment volumes in radiation therapy treatment planning. Manual delineation is challenging owing to difficulties in discriminating the edges of malignant lesions from noisy PET images in addition to being operator-dependent and sensitive to high inter- and intra-observer variability. Consequently, a considerably large number of strategies have been proposed for semi-automated or fully automated segmentation of metabolically active lesions and other organs/tissues from PET images.[80, 81] These techniques have been classified in a number of categories including thresholding, gradient-based, region growing and adaptive region growing, statistical, learning and texture-based segmentation, or algorithms combined with image processing and/or reconstruction or incorporated in multimodality image segmentation framework.[81] A selection of these algorithms, particularly those that require no or little interaction with the users, have been used with

Figure 6. Illustration of the basic foundations of PET quantification and the factors involved in the calculation of first- and second-order image-derived PET metrics used in clinical oncology. PET, positron emission tomography.

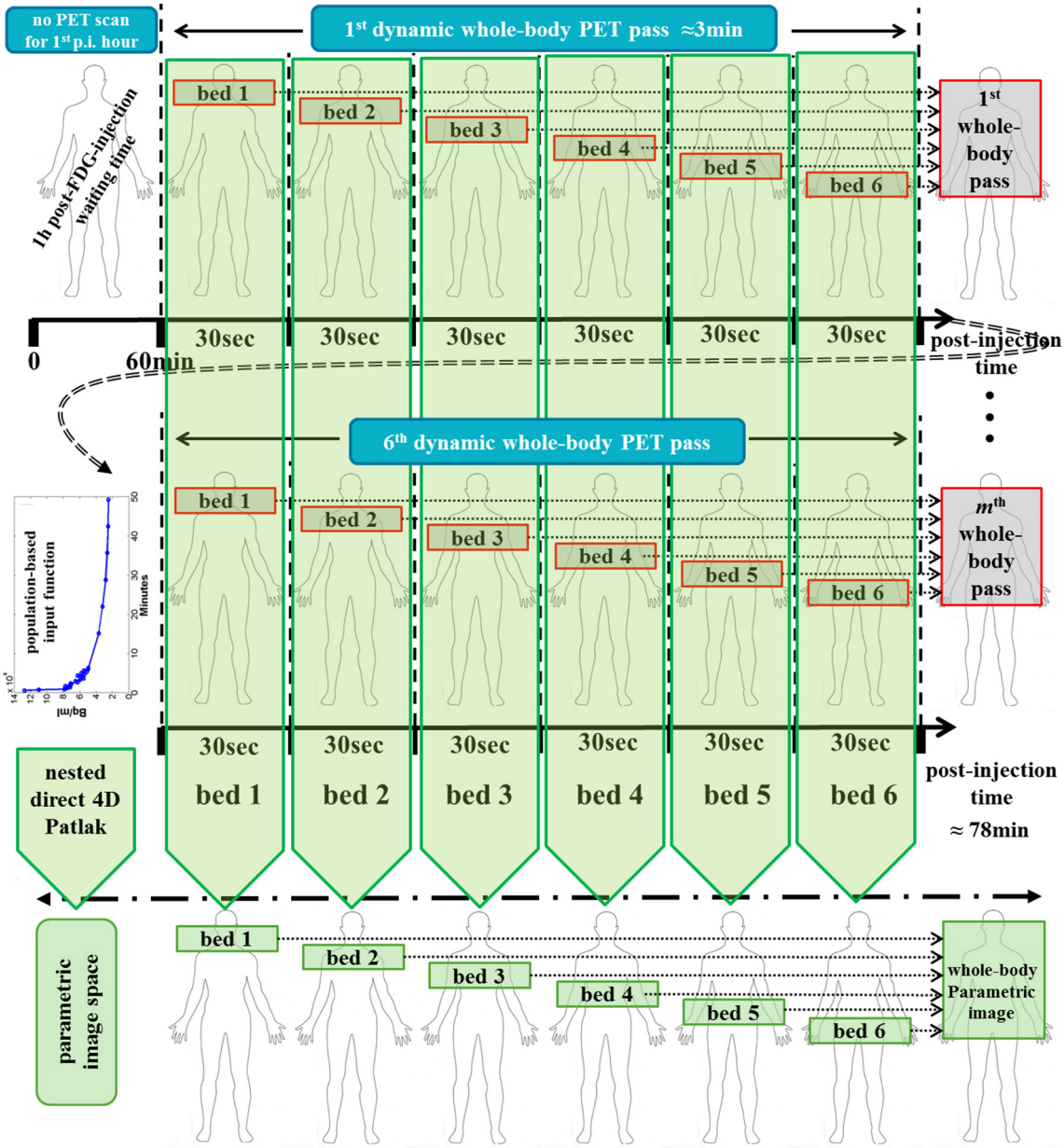


limited success for the assessment of MTVs and metabolic activity for one of the two applications mentioned earlier, that is, monitoring response to treatment or radiation treatment planning. A major challenge facing the development and comparative evaluation of PET image segmentation techniques is the absence of standardized metrics and a benchmark for the objective evaluation of their accuracy. This challenge has recently been addressed by the American Association of Physicists in Medicine Task Group 211 who devised various strategies to evaluate the accuracy of PET image segmentation techniques through simulation and experimental phantom studies and pathology-validated clinical datasets.[82] Continuation of this effort will hopefully facilitate the translation and application of advanced segmentation approaches in clinical settings.

## High-order metrics: radiomics (texture analysis)

Despite the widespread adoption in the clinic and popularity of the above-discussed PET metrics, there is clearly a need in PET quantification, which led to the proposal of more advanced concepts based on powerful statistical approaches. Pioneering studies demonstrated solid evidence that meaningful information can be derived from PET images to guide the identification of explicit markers linked to tumour molecular and genetic profiles.[83]

In this regard, radiomics[84] and texture analysis[85] emerged as novel and promising approaches having the potential to overcome the limitations of conventional approaches by providing

reliable prognostic information with a high predictive power in a number of malignancies. Texture analysis[85] emerged as a new technique allowing the analysis of metabolic intratumoural tracer uptake heterogeneity in malignant lesions.[85–88] A number of studies reported on the correlation between therapy outcome and metrics derived by advanced image processing techniques, all of them showing that texture features outperform commonly used SUV-based descriptors.[89–91] The approach holds the promise of extracting useful textural features from PET images to substantially facilitate prognosis in solid tumours.

As a consequence of the progress in quantitative imaging and the emergence of systems biology, a new research domain emerged referred to as radiomics.[84] Radiomics is defined as the science of correlating statistical data pulled out from multimodal medical images with tumour biology and the clinical picture of the patient to enhance the predictive power of multimodality molecular imaging. This description is linked to the ultimate radiomics hypothesis that "*tissue characteristics at the molecular level are reflected in macroscopic features of medical images and, therefore, an advanced quantitative analysis can infer genomics and proteomics patterns, possibly containing prognostic information*".[92] Despite the fact that this approach is still in an embryonic state, an ample number of pioneering studies have been published in the scientific literature supporting this hypothesis. Yet, further research and development efforts as well as large patient databases for different oncological indications are needed to fully characterize the robustness, reliability and limitations before the technique can be adopted in clinical setting.[84, 93]

### Parametric imaging

Parametric imaging emerged as a promising approach in clinical oncology enabling the generation of quantitative maps representing physiological parameters derived through dynamic PET data acquisition and kinetic modelling. The approach had been initially studied only in the context of single-bed FOV imaging and demonstrated improved accuracy in discriminating benign from malignant disease, when combined with discriminant analysis.[94] However, single-bed dynamic scans require a priori knowledge of the region containing the metabolic abnormalities to ensure the selected bed position covers it adequately and, as such, has limited capability in evaluating distant disease, such as metastasis, spread throughout the body. These shortcomings have been addressed recently by a proposed class of 4D WB PET imaging methods, designed for efficient tracking of the spatiotemporal map of the PET signal across multiple beds. The acqu ired PET dataset can then facilitate the WB parametric imaging of the tracer uptake macro-parameters, such as that of net uptake rate $K_i$ and total blood volume distribution $V$, in order to ultimately translate the quantitative virtues of dynamic PET in WB FOVs and to clinical oncology.[22, 60] The support for parametric PET images, beyond the currently established semi-quantitative SUV metric, may be useful in clinical oncology: for multiparametric evaluations of metastatic tumours across multiple beds as well as for improved reproducibility and treatment response assessments over long periods. These protocols are designed to exploit the inherent 4D spatiotemporal nature of the complete list-mode PET data.[95]

In Table 1, we present an overview of the range of quantitative PET imaging methods discussed in this review that could benefit clinical oncology studies. More specifically, we summarize, for each referenced class of methods, its associated set of image metrics, scope of definition, advantages and limitations, accuracy and precision of the respective parametric images as well as current and potential future applications and implementation status in the domain of clinical oncology.

## ADVANCED STRATEGIES FOR INDIRECT AND DIRECT PARAMETRIC WHOLE-BODY IMAGING

Parametric PET imaging involves the spatiotemporal or dynamic (4D) acquisition of the administered PET tracer activity distribution to produce quantitative images of physiological parameters of high quantitative value and potentially significant clinical interest, beyond the well-established and widely adopted in the clinic SUV metric.[96] Naturally, dynamic PET imaging segments the total amount of acquired PET data into a set of time frames. Assuming a limited total PET scan time, as currently dictated by the clinical need for high patient throughput and relatively short scan periods, the expected statistical noise levels in each dynamic PET frame may considerably increase with the number of frames. Moreover, the noise is expected to further increase when the limited total scan time is segmented not only across multiple temporal frames but also over multiple bed positions.[68 22, 60]

In general, parametric PET imaging methods can be classified into two general categories, depending on the PET data representation level at which they are applied. The first class, often denoted as indirect parametric imaging methods, includes all methods applied on the independently reconstructed dynamic PET images of each bed position to indirectly derive the respective parametric images.[22] In contrast, the second class, known as direct 4D parametric imaging methods[70] ,[73] involves statistical iterative image reconstruction algorithms that incorporate the graphical analysis or compartmental model assumptions into the reconstruction's response model and directly utilize the available 4D PET projection data from all dynamic frames of each bed position to estimate the tracer kinetic parameters .

Indirect parametric imaging methods are relatively simpler to implement and can be retrospectively applied to any available set of dynamic PET images since the respective scan time information per frame is usually embedded in the frame data. However, post-reconstruction parametric analysis can pose certain quantitative limitations. In particular, each of the dynamic PET images later analysed by indirect algorithms is exclusively reconstructed from the data of a single dynamic PET frame, which in modern dynamic PET protocols may involve very short time periods and thus elevated levels of statistical noise. As a result, even if the high data noise levels are limited to only one or few of the frames, they are naturally propagated into the respective images, through the low-count 3D frame-by-frame independent reconstructions, and further into the parametric images, through the indirect statistical regression estimation process.[71] In fact, a complementary frame reconstruction method has been recently proposed

Table 1. Overview of the basic classes of quantitative PET imaging methods applicable to clinical oncology

| Quantitative method | Metric | Definition/Scope | Advantages | Limitation | Accuracy | Precision | Oncology applications | Implementation status |
|---|---|---|---|---|---|---|---|---|
| First-order static | $SUV_{max}$<br>$SUV_{peak}$ | Time-averaged uptake account for dose and (lean) body mass | Simplified acquisition, established in the clinic, applicable to low counts | Semi-quantitative, $SUV_{max}$ can be highly sensitive to noise | Post-injection time-dependent, neglecting blood plasma activity & tumour metabolic volume | $SUV_{max}$: low in regions of low uptake | Standard-of-care & research clinical scan protocols | Completed, widely employed and supported |
| Second-order (post region delineation) static | $SUV_{mean}$<br>MTV<br>TLG | Time- and space-averaged uptake, accounts for dose, body mass and metabolic tumour volume | Simplified, adoptable, applicable to low counts, relevant to metabolic tumour volume | Semi-quantitative, highly dependent on tumour delineation and PVE | Time- and segmentation-dependent, neglecting blood plasma activity | Moderate due to high dependence on tumour delineation and PVE | Widely employed in clinical research, but not yet standard-of-care, promising for tumour staging | Ongoing development of automated robust tumour delineation & segmentation methods |
| Third-order (radiomics) static | Texture uptake features | Low- and high-order texture and heterogeneity uptake features | Quite large variety of features high predictive power for malignancy capable of assessing heterogeneous uptake features | Potentially large intercorrelations between a wide set of features requires sufficiently high uptake contrast and number of tumour voxels | Limited accuracy depending on resolution, number of intratumour voxels and number of counts/voxels, sensitive to PVE and tumour delineation | Highly variable precision depending on the order of the evaluated texture feature | Demonstrated correlation between therapy outcome and certain texture features, enhanced prognosis of malignant tumours | Recently emerged, extensive validation and machine/deep learning developments required |
| Simplified kinetic analysis | Dual-time point: $SUV_{ratio}$ *or* simplified $K_i$ assuming known $V$ macro-parameter | Relevant SUV difference based on two dynamic frames $K_i$ evaluation on ROIs only after taking plenty of kinetic assumptions | Simplified, adoptable, robust (linear models) applicable even for very few (two) dynamic frames per bed or in the absence of input function | Relies on too many kinetic assumptions, ROI-based analysis only, requires a priori knowledge of macro-parameters, very limited clinical usefulness | Quite limited accuracy due to too many assumptions, dual-time image analysis highly dependent on the selected acquisition time window | Robust precise ROI-based macro-parameter estimates thanks to linear modelling | Very limited applications in $^{18}$F-FDG and $^{18}$F-NaF (sodium fluoride) tumour imaging | Completed for dynamic ROI-based analysis of specific types of malignancies, extensive clinical validation required for each of the taken kinetic assumptions |

(Continued)

Table 1. (Continued)

| Quantitative method | Metric | Definition/Scope | Advantages | Limitation | Accuracy | Precision | Oncology applications | Implementation status |
|---|---|---|---|---|---|---|---|---|
| Dynamic (low-order) graphical analysis | Kinetic macro-parameters Patlak ($K_i$, $V$, $k_{loss}$) Logan ($DV$) accounting for the input function | Kinetic macro-parameters imaging (net uptake rate, distribution volume, etc.) taking only few assumptions, may offer highly quantitative imaging of a summary of kinetic uptake attributes at high precision, beyond SUV, and across WB FOVs | Adoptable even for WB dynamic scans, linearized robust voxel-based imaging of clinically relevant macro-parameters, Patlak class suitable for WB parametric imaging direct-4D graphical analysis associated with high precision linear methods applicable in theory even for two dynamic frames, most preferred parametric imaging class of methods in clinical practice | Model assumptions valid only after a certain post-injection time, robust linear sPatlak does not account for uptake reversibility ($k_4 > 0$), linearized gPatlak accounts for mild reversibility as well (small positive $k_4$) but not very robust | Highly accurate provided reasonable temporal sampling rate and validity of model assumptions, Logan $DV$ accuracy relies on fine temporal sampling of early uptake, sPatlak under-estimates $K_i$ if true $k_4 > 0$ especially at later times, gPatlak may achieve high $K_i$ accuracy regardless of zero or mildly positive $k_4$ and scan time window, potential errors in parameter estimates may propagate beyond their origin with direct 4D imaging | Single-bed dynamic: high precision in parametric images, WB dynamic: moderate (indirect) to high (direct-4D) precision, sPatlak achieved higher precision than gPatlak when applied indirectly, sPatlak and gPatlak direct-4D algorithms exhibited similar precision levels, in terms of CNR detectability, gPatlak achieved higher scores for tumours with non-negligible uptake reversibility | Applicable to both single-bed but most importantly WB dynamic PET imaging protocols (the latter with Patlak methods), WB Patlak $^{18}$F-FDG imaging demonstrated improved tumour detectability in the liver and thorax, WB gPatlak $^{18}$F-FDG imaging exhibited further detectability enhancement in tumours with mild uptake reversibility (hepato-cellular carcinomas), clinical application of combined SUV/Patlak imaging demonstrated potential of multiparametric $^{18}$F-FDG PET in oncology | Completed for both indirect and direct 4D imaging for most graphical analysis methods employed in oncology research studies, clinically adoptable indirect and 4D WB Patlak imaging algorithms implemented in clinical setting in academic and corporate settings, ongoing clinical validation of specific features of hybrid SUV/Patlak $^{18}$F-FDG imaging algorithms: population-based image-derived input function & synthesis of SUV PET images from the dynamic WB PET data |

(Continued)

Table 1. (Continued)

| Quantitative method | Metric | Definition/Scope | Advantages | Limitation | Accuracy | Precision | Oncology applications | Implementation status |
|---|---|---|---|---|---|---|---|---|
| Dynamic compartment (high-order) full kinetic modelling | Kinetic microparameters ($K_1$, $k_2$, $k_3$ and $k_4$) accounting for the input function | Kinetic microparameter imaging (uptake rate constants) taking minimum kinetic assumptions, may offer highly quantitative detailed information, in addition to SUV, but only for a selected single bed position | Highly accurate estimation of the fine kinetic features of tracers' dynamic uptake, most accurate parametric imaging methods (specialists best friend) | Not very robust to high PET data noise levels due to non-linear estimation of a large number of kinetic parameters, sensitive to noise-induced bias, not possible for multibed kinetic analysis, nevertheless single-bed fully kinetic modelling can be combined with multibed Patlak imaging | Highly accurate at moderate noise levels, potential noise-induced bias at PET data high noise levels, potential errors in parameter estimates may propagate beyond their origin with direct 4D imaging | Moderate to low precision in parametric images even with direct-4D imaging due to non-linear modelling | Full kinetic modelling applied in clinical research studies for specific type of tumours and tracers (primarily $^{18}$F-FDG), demonstrated improved tumour detectability, potential utilization for the identification of benign and malignant tumours | Basic implementation of variants of compartmental kinetic modelling analysis (with 1 or 2-tissue compartments) have been completed but with very limited clinical validation for only specific types of malignancy and tracers (primarily $^{18}$F-FDG) |

CNR, contrast-to-noise ratio; 4D, four-dimensional; FOV, field-of-view; MTV, metabolic active volume; PET, positron emission tomography; PVE, partial volume effect; ROI, region of interest; SUV, standardized uptake value; TLG, total lesion glycolysis; WB, whole -body.

to avoid propagation of the very high noise levels of very short dynamic PET frames into the respective images.[97]

Nevertheless, regardless of the reconstruction method, the underlying statistical noise in each of the dynamic PET images follows a complex mixture of Gaussian distributions, due to the intervoxel correlations introduced by the reconstruction process. Indirect parametric imaging methods are forced to model this highly correlated noise, as they are designed to operate on the dynamic image space. Consequently, indirect methods end up only approximating the noise distribution of their input images, thus increasing the likelihood for noise-induced quantitative errors in the final parametric images.[71]

On the other hand, direct 4D parametric reconstruction algorithms embed the employed kinetic model response into a dynamic PET image reconstruction algorithm. Thus, the effect of the tracer pharmacokinetic properties on the dynamic course of the PET activity concentration can be accounted for at every voxel during the dynamic PET image reconstruction process. The kinetic model may be incorporated either as an additional modelling component of the system matrix, if the properties of the selected kinetic analysis method permit so, or more generally, as a nested iterative reconstruction routine within each iteration step of the frame-by-frame dynamic PET tomographic reconstruction method for accelerated convergence.[71, 98]

Moreover, direct 4D parametric imaging utilizes all available PET data from all dynamic frames of a bed position to reconstruct the parametric images for that bed. As a result, the propagated noise from the data to the parametric images is now determined by the total amount of 4D data per bed, rather than per frame per bed, thereby resulting in considerably less amounts of noise in the final parametric images.[99] In fact, the degree of noise suppression in 4D parametric imaging is expected to be more profound, relative to indirect imaging, for acquisitions involving limited amounts of data per bed where higher levels of statistical noise are expected in general. Therefore, direct 4D parametric methods becomes more vital in WB dynamic PET imaging protocols, to avoid high noise levels and potential noise-induced quantitative errors in the respective WB parametric images. Furthermore, the 4D parametric reconstruction methods are directly applied on the PET projection data where the noise follows the well-defined Poisson distribution that can be accurately modelled to avoid noise-induced bias and retain the high quantitative value of the WB parametric images.[71] Recently, the quantitative benefits of direct 4D WB parametric imaging in clinical oncology have been demonstrated by a study showing improved tumour detectability and contrast after utilizing a robust family of nested direct 4D WB (s/g)Patlak reconstruction methods(Figure 7).[71]

As mentioned earlier, motion during acquisition can be a major problem for resolution and quantification, especially in WB imaging where it is highly variable and non-rigid in nature, compared to the brain. In addition, WB parametric imaging may be particularly sensitive to motion, as 4D WB PET data are susceptible not only to intra- but also inter-frame non-rigid

Figure 7. (Top rows) Transaxial and coronal slices of WB $^{18}$F-FDG PET SUV (left three columns) and Patlak $K_i$ (right three columns) images as reconstructed from dynamic WB $^{18}$F-FDG PET data of a clinical oncology case over a 10–45 min post-injection scan time window. The first column refers to a post-reconstruction smoothed [Gaussian full width at half maximum (FWHM) of 5 mm] WB PET SUV image from the same case as acquired from a past single-pass WB PET standard-of-care scan 1 month before the respective dynamic WB PET exam study. (Bottom rows): Quantitative ROI analysis of the TBR and CNR scores for different number of Maximum Likelihood Expectation Maximisation (MLEM) iterations over a liver and chest suspected tumour ROIs demonstrating the enhanced quantification, contrast and detectability attained with parametric $K_i$ imaging over SUV particularly for direct 4D $K_i$ imaging methods. In addition, gPatlak 4D $K_i$ imaging is associated with the highest contrast, although background $K_i$ signal is also enhanced in many regions, thereby confirming gPatlak superior quantitative performance compared to respective sPatlak 4D $K_i$ imaging.

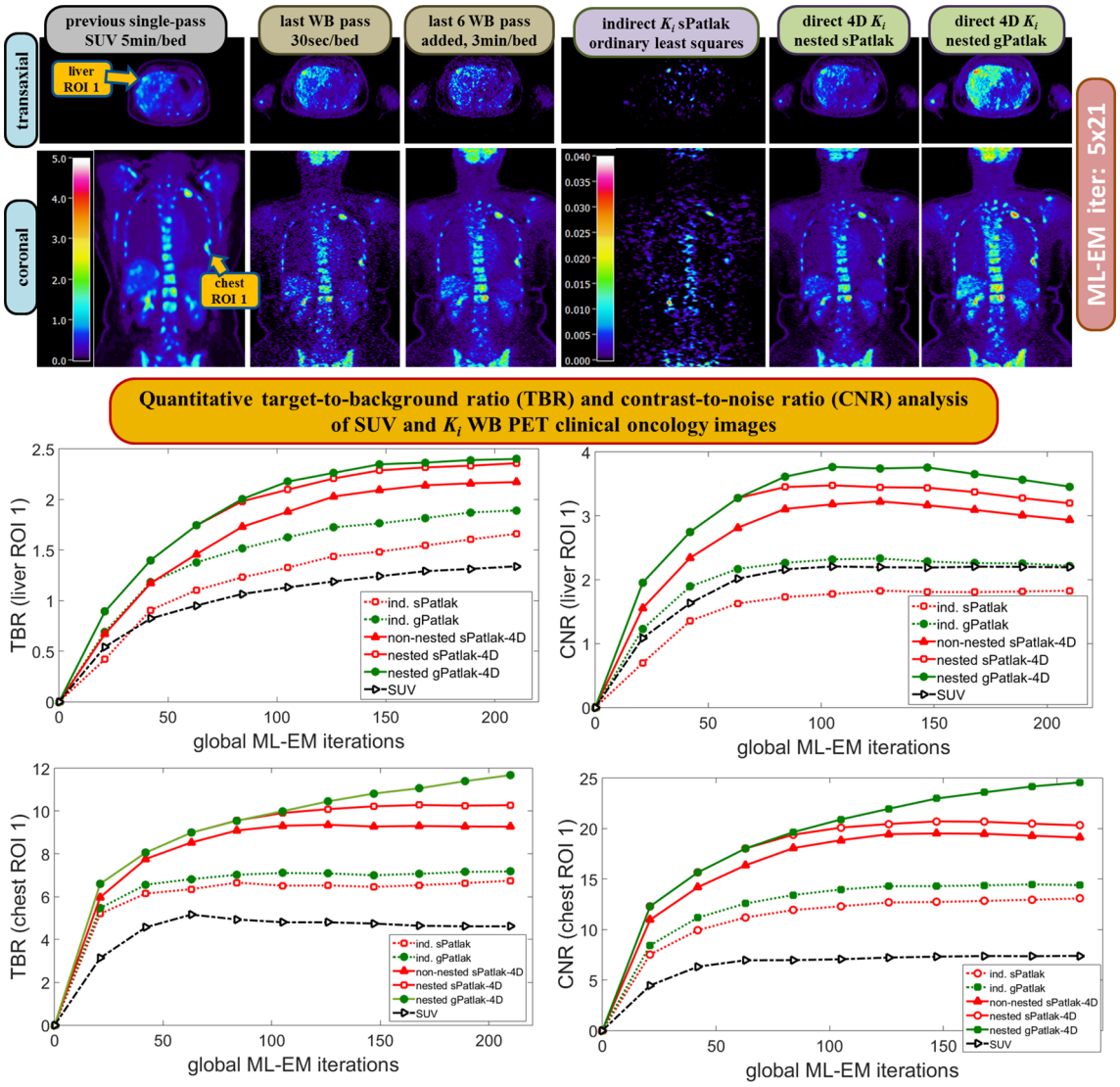


motion at each bed position. A recently proposed nested iterative Richardson-Lucy (RL) motion compensated image reconstruction (MCIR) algorithm permitted the accelerated iterative deconvolution of the motion within each dynamic PET image, prior to parametric imaging, .[50] The preliminary evaluation of this technique with realistic simulations demonstrated significant resolution and contrast recovery in tumour lesions in both the motion-compensated dynamic PET and the respective $K_i$ images with and without presence of noise (Figure 8). However, it also revealed distinct Gibbs artefacts in the final images, even in the absence of noise, owing to the correlations induced due to the iterative deconvolution process (Figure 8 - top panel). Comparable observations were reported in the presence of moderately high levels of noise, particularly in areas with low tracer uptake (Figure 8 - middle panel). Yet, both the artifacts and the noise had little impact on the improved tumour lesion detectability and CNR scores attained with motion-compensated dynamic PET image reconstructions.

Temporally continuous dynamic PET data are currently only feasible for single-bed dynamic PET acquisitions, owing to the limited axial FOV of present clinical PET scanners. Therefore, full

Figure 8. (Top panel): Noise-free last dynamic PET SUV (top) and sPatlak images (bottom) corresponding to a simulated clinical WB dynamic cardiac PET acquisition. In all cases, motion-free, ground truth 4D data (first column) are used as a reference to compare against motion contaminated data estimated without motion correction (second column) and with nested RL-3D-MCIR correction (third column). All SUV PET images were reconstructed after 4 × 21 MLEM global iterations.Moreover, 10 nested RL subiterations were performed within each global iteration of the RL-3D-MCIR method. (Middle panel): Same dynamic PET (top) and sPatlak $K_i$ images (bottom), after adding quantitative levels of Poisson noise on projection space, equivalent to 45 sec per bed frame and scaling to match the reported sensitivity performance of Siemens Biograph™ mCT PET/CT scanner. (Bottom panel): CNRs for lung tumour as drawn on the PET SUV images (dotted curves) corresponding to the sixth dynamic frame and the respective sPatlak $K_i$ images (continuous curves). The tumour CNR performance scores in the motion-compensated images with the proposed nested RL-3D-MCIR method (red squares) are evaluated against the simulated motion-free ground truth images (blue circles) and the uncorrected for motion images (green triangles ) of the SUV (empty markers) and Ki (filled markers) metrics. 4D, four-dimensional; MCIR, motion compensated image reconstruction; RL, Richardson-Lucy; 3D, three-dimensional.

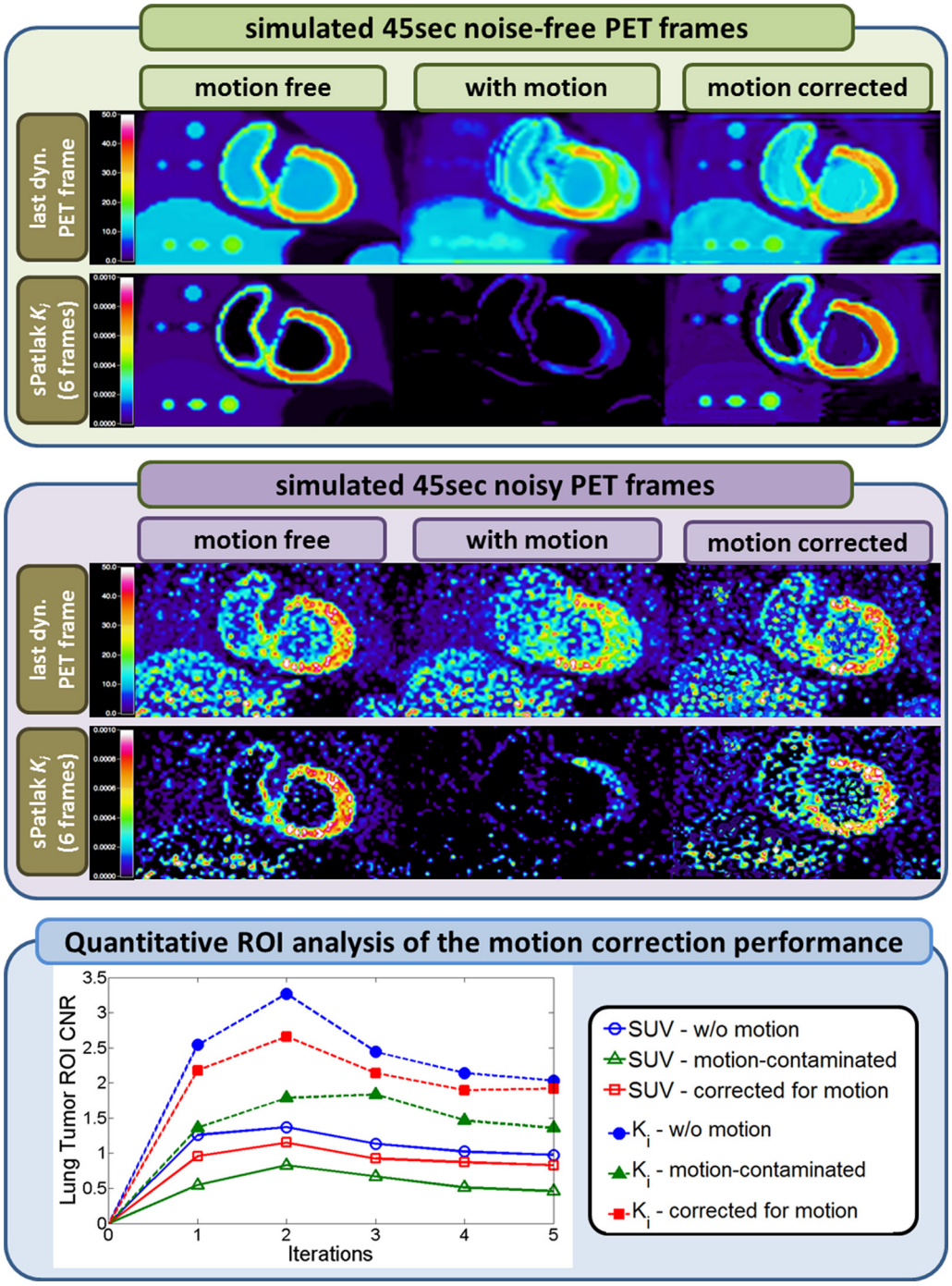

compartmental modelling methods remain confined to single bed FOVs , which limits their adoptability in clinical oncology. More recently, a modified CBM WB dynamic protocol was proposed aiming at full compartmental modelling in a targeted single bed FOV covering a mediastinal blood pool region, such as the heart or the aorta, while sPatlak analysis is performed across all bed positions.[100] The preliminary clinical evaluation suggested that $K_i$ images can be indirectly produced by microparameters through compartmental modeling at a selected single bed position, in addition to WB $K_i$ parametric images directly estimated with Patlak graphical analysis methods, after using a clinically feasible dynamic PET imaging protocol.[100] In the future, the advent of total-body PET scanners may allow the deployment of fully compartmental WB parametric imaging techniques with standard dosages as well as robust Patlak WB imaging methods with ultra-low dosages.[101]

## CONCLUDING REMARKS AND FUTURE PROSPECTS

PET is currently established in clinical oncology as a molecular imaging modality capable of quantitatively characterizing, with relevantly high sensitivity and specificity, the physiological activity of a spectrum of major biochemical mechanisms underlying normal and tumour tissues.[21] A significant portion of the PET clinical value lies in its inherent quantitative nature, stemming from the ability to measure the spatiotemporal distribution of independent quantifiable counts originating from a wide range of radiolabelled biomarkers.

However, a number of factors, including physics processes, hardware specifications, modelling algorithms and scan protocol features, may affect the quantification of the static and parametric PET images. In addition, the interpretation of the PET images analysis can significantly vary depending on the specific image metric evaluated.

The ultimate mission of PET imaging in clinical oncology is the extraction of clinically relevant, accurate, precise and reproducible information for specific molecular mechanisms underlying tumour physiology to improve the diagnosis, staging and treatment response assessments of primary and metastatic oncological malignancies. PET modality offers the unique capability to image the physiological progress of many major biochemical processes underlying different types of malignancy. Nevertheless, its clinical power lies primarily in its inherent capability to obtain quantitative measurements that enable the numerical objective analysis of the PET images in order to extract reliable and reproducible information for the diagnosis, staging and therapy planning of oncological primary and metastatic lesions. Thus, preserving as well as further enhancing PET quantification value can be crucial for oncological imaging.

The current technological trends in PET imaging, including the advent of simultaneous PET/MR clinical systems, fast TOF timing resolution, task-dependent resolution modelling, direct 4D reconstruction, WB parametric imaging, continuous bed motion and total body PET systems, indicate a clear trend for significant enhancements in PET sensitivity and modelling capabilities for the near future. Ultra-fast WB dynamic PET acquisitions with efficient list-mode direct 4D reconstruction methods for the accurate event-driven compensation of a variety of PET quantification degradation factors may soon become available in clinic. Finally, the current state-of-the art PET systems technology already permits the exploitation of the intrinsic spatiotemporal list-mode nature of the PET data coupled with the CBM acquisition mode to provide multiparametric and quantitative WB PET imaging assessments beyond the SUV. A clinically adoptable hybrid SUV/$K_i$ PET imaging framework may ultimately pave the way for the translation of the PET quantitative virtues into the clinic and become the next standard-of-care paradigm in clinical oncology.

The advent in the clinic of TOF acquisition with constantly improving time resolution, the optimization of resolution modelling reconstruction methods and the introduction of direct 4D WB parametric PET image reconstruction algorithms can pave the way for the translation of the full quantitative PET virtues into clinical oncology. The design of clinically adoptable 4D WB PET imaging protocols supporting both the conventional SUV and the advanced macro-kinetic parameters of high clinical relevance, such as the $K_i$ influx rate constant, may significantly enhance the molecular information content delivered in routine clinic for more reliable diagnostic, prognostic and theranostic assessments in oncology.

## ACKNOWLEDGEMENTS

This work was supported by the Swiss National Science Foundation under grant No. SNSF 320030_176052 and the Swiss Cancer Research Foundation under Grant KFS-3855-02-2016.

## REFERENCES

1. Czernin J, Allen-Auerbach M, Schelbert HR. Improvements in cancer staging with PET/CT: literature-based evidence as of September 2006. *J Nucl Med* 2007; **48**(Suppl 1): 78S–88.
2. Karakatsanis N, Bao Q, Vu N, Chatziioannou A .Investigation of the minimum detectable activitylevel of a preclinical LSO PET scanner IEEE Nuclear Science Symposium Conference Record. 2007: 3133-3138
3. Efthimiou N, Loudos G, Karakatsanis NA, Panayiotakis GS. Effect of 176Lu intrinsic radioactivity on dual head PET system imaging and data acquisition, simulation, and experimental measurements. *Med Phys* 2013; **40**: 112505: 112505: . doi: https://doi.org/10.1118/1.4824694
4. Bentourkia M, Zaidi H. Tracer kinetic modeling in PET. *PET Clin* 2007; **2**: 267–77. doi: https://doi.org/10.1016/j.cpet.2007.08.003
5. Muzi M, O'Sullivan F, Mankoff DA, Doot RK, Pierce LA, Kurland BF, et al. Quantitative assessment of dynamic PET imaging data in cancer imaging. *Magn Reson Imaging* 2012; **30**:

1203–15. doi: https://doi.org/10.1016/j.mri.2012.05.008
6. Zaidi H, Becker M. The promise of hybrid PET\/MRI: technical advances and clinical applications. *IEEE Signal Process Mag* 2016; **33**: 67–85. doi: https://doi.org/10.1109/MSP.2015.2482225
7. Kumar R, Dhanpathi H, Basu S, Rubello D, Fanti S, Alavi A. Oncologic PET tracers beyond 18FFDG and the novel quantitative approaches in PET imaging. *Q J Nucl Med Mol Imaging* 2008; **52**: 50–65.
8. Jamar F, Buscombe J, Chiti A, Christian PE, Delbeke D, Donohoe KJ, et al. EANM/SNMMI guideline for $^{18}$F-FDG use in inflammation and infection. *J Nucl Med* 2013; **54**: 647–58. doi: https://doi.org/10.2967/jnumed.112.112524
9. Sun X, Niu G, Chan N, Shen B, Chen X. Tumor hypoxia imaging. *Mol Imaging Biol* 2011; **13**: 399–410. doi: https://doi.org/10.1007/s11307-010-0420-z
10. Lin FI, Rao JE, Mittra ES, Nallapareddy K, Chengapa A, Dick DW, et al. Prospective comparison of combined $^{18}$F-FDG and $^{18}$F-NaF PET/CT vs. $^{18}$F-FDG PET/CT imaging for detection of malignancy. *Eur J Nucl Med Mol Imaging* 2012; **39**: 262–70. doi: https://doi.org/10.1007/s00259-011-1971-1
11. Zaidi H, Alavi A. Trends in PET quantification: opportunities and challenges. *Clin Transl Imaging* 2014; **2**: 183–5. doi: https://doi.org/10.1007/s40336-014-0065-z
12. Acton PD, Zhuang H, Alavi A. Quantification in PET. *Radiol Clin North Am* 2004; **42**: 1055–62. doi: https://doi.org/10.1016/j.rcl.2004.08.010
13. Huang SC. Anatomy of SUV. Standardized uptake value. *Nucl Med Biol* 2000; **27**: 643–6.
14. Patlak CS, Blasberg RG. Graphical evaluation of blood-to-brain transfer constants from multiple-time uptake data. Generalizations. *J Cereb Blood Flow Metab* 1985; **5**: 584–90. doi: https://doi.org/10.1038/jcbfm.1985.87
15. Wahl RL, Jacene H, Kasamon Y, Lodge MA. From RECIST to PERCIST: Evolving considerations for PET response criteria in solid tumors. *J Nucl Med* 2009; **50**(Suppl1): 122S–50. doi: https://doi.org/10.2967/jnumed.108.057307
16. Zaidi H. eds. *Quantitative analysis in nuclear medicine imaging*. New York: Springer; 2006
17. Basu S, Zaidi H, Houseni M, Bural G, Udupa J, Acton P, et al. Novel quantitative techniques for assessing regional and global function and structure based on modern imaging modalities: implications for normal variation, aging and diseased states. *Semin Nucl Med* 2007; **37**: 223–39. doi: https://doi.org/10.1053/j.semnuclmed.2007.01.005
18. Weber WA, Schwaiger M, Avril N. Quantitative assessment of tumor metabolism using FDG-PET imaging. *Nucl Med Biol* 2000; **27**: 683–7. doi: https://doi.org/10.1016/S0969-8051(00)00141-4
19. Houshmand S, Salavati A, Hess S, Werner TJ, Alavi A, Zaidi H. An update on novel quantitative techniques in the context of evolving whole-body PET imaging. *PET Clin* 2015; **10**: 45–58. doi: https://doi.org/10.1016/j.cpet.2014.09.004
20. Boellaard R. Need for standardization of $^{18}$F-FDG PET/CT for treatment response assessments. *J Nucl Med* 2011; **52**(Suppl 2): 93S–100. doi: https://doi.org/10.2967/jnumed.110.085662
21. Bai B, Bading J, Conti PS. Tumor quantification in clinical positron emission tomography. *Theranostics* 2013; **3**: 787–801. doi: https://doi.org/10.7150/thno.5629
22. Karakatsanis NA, Lodge MA, Tahari AK, Zhou Y, Wahl RL, Rahmim A. Dynamic whole-body PET parametric imaging: I. Concept, acquisition protocol optimization and clinical application. *Phys Med Biol* 2013; **58**: 7391–418. doi: https://doi.org/10.1088/0031-9155/58/20/7391
23. Conti M. Focus on time-of-flight PET: the benefits of improved time resolution. *Eur J Nucl Med Mol Imaging* 2011; **38**: 1147–57. doi: https://doi.org/10.1007/s00259-010-1711-y
24. Rahmim A, Qi J, Sossi V. Resolution modeling in PET imaging: theory, practice, benefits, and pitfalls. *Med Phys* 2013; **40**: 064301–15. doi: https://doi.org/10.1118/1.4800806
25. Reader AJ, Zaidi H. Advances in PET image reconstruction. *PET Clin* 2007; **2**: 173–90. doi: https://doi.org/10.1016/j.cpet.2007.08.001
26. Zaidi H, Hasegawa B. Determination of the attenuation map in emission tomography. *J Nucl Med* 2003; **44**: 291–315.
27. Kitamura H, Inoue K, Sasaki T, Tsuda K, Fujimori H, Tanaka T, et al. Estimation of local statistical noise in PET images induced by attenuation inside the body. *Ann Nucl Med* 2010; **24**: 197–205. doi: https://doi.org/10.1007/s12149-010-0355-0
28. Kinahan PE, Hasegawa BH, Beyer T. X-ray-based attenuation correction for positron emission tomography/computed tomography scanners. *Semin Nucl Med* 2003; **33**: 166–79. doi: https://doi.org/10.1053/snuc.2003.127307
29. Mehranian A, Arabi H, Zaidi H. Vision 20/20: magnetic resonance imaging-guided attenuation correction in PET/MRI: challenges, solutions, and opportunities. *Med Phys* 2016; **43**: 1130–55. doi: https://doi.org/10.1118/1.4941014
30. Arabi H, Zaidi H. One registration multi-atlas-based pseudo-CT generation for attenuation correction in PET/MRI. *Eur J Nucl Med Mol Imaging* 2016; **43**: 2021–35. doi: https://doi.org/10.1007/s00259-016-3422-5
31. Defrise M, Rezaei A, Nuyts J. Time-of-flight PET data determine the attenuation sinogram up to a constant. *Phys Med Biol* 2012; **57**: 885–99. doi: https://doi.org/10.1088/0031-9155/57/4/885
32. Mehranian A, Zaidi H. Joint estimation of activity and attenuation in whole-body TOF PET/MRI using constrained gaussian mixture models. *IEEE Trans Med Imaging* 2015; **34**: 1808–21. doi: https://doi.org/10.1109/TMI.2015.2409157
33. Robson PM, Dweck MR, Trivieri MG, Abgral R, Karakatsanis NA, Contreras J, et al. Coronary artery PET/MR imaging: feasibility, limitations, and solutions. *JACC Cardiovasc Imaging* 2017; **10**(10 Pt A(). doi: https://doi.org/10.1016/j.jcmg.2016.09.029
34. Karakatsanis N, Robson P, Dweck M, Abgral R, Trivieri M, Sanz J. MR-based attenuation correction in cardiovascular PET/MR imaging: challenges and practical solutions for cardiorespiratory motion and tissue class segmentation. *J Nucl Med* 2016; **57**(suppl 2): 452.
35. Zaidi H, Koral KF. Scatter modelling and compensation in emission tomography. *Eur J Nucl Med Mol Imaging* 2004; **31**: 761–82. doi: https://doi.org/10.1007/s00259-004-1495-z
36. Iatrou M, Manjeshwar RM, Wollenweber SD, Ross SG, Stearns CW, IEEE. 2009. Out-of-field scatter estimation in 3D whole body PET. Orlando, FL, USA: IEEE Nuclear Science Symposium Conference Record. 3886–8
37. Levin CS, Hoffman EJ. Calculation of positron range and its effect on the fundamental limit of positron emission tomography system spatial resolution. *Phys Med Biol* 1999; **44**: 781–99. doi: https://doi.org/10.1088/0031-9155/44/3/019
38. Soultanidis G,Karakatsanis N,Nikiforidis G,Loudos G. 2011 Study of the effect of magnetic field inpositron range using GATE simulation toolkitJournal of Physics: Conference Series Vol 317 No. 1012021
39. Shibuya K, Yoshida E, Nishikido F, Suzuki T, Tsuda T, Inadama N, et al. Annihilation photon acollinearity in PET: volunteer and phantom FDG studies. *Phys*

*Med Biol* 2007; **52**: 5249–61. doi: https://doi.org/10.1088/0031-9155/52/17/010
40. Mizuta T, Kitamura K, Ishikawa A, Ohtani A, Tanaka K. A scatter-compensated crystal interference factor in component-based normalization for high-resolution whole-body PET. *Phys Med Biol* 2010; **55**: 3643–57. doi: https://doi.org/10.1088/0031-9155/55/13/005
41. Shao Y, Sun X, Lan KA, Bircher C, Lou K, Deng Z. Development of a prototype PET scanner with depth-of-interaction measurement using solid-state photomultiplier arrays and parallel readout electronics. *Phys Med Biol* 2014; **59**: 1223–38. doi: https://doi.org/10.1088/0031-9155/59/5/1223
42. Rousset O, Rahmim A, Alavi A, Zaidi H. Partial volume correction strategies in PET. *PET Clin* 2007; **2**: 235–49. doi: https://doi.org/10.1016/j.cpet.2007.10.005
43. Erlandsson K, Buvat I, Pretorius PH, Thomas BA, Hutton BF. A review of partial volume correction techniques for emission tomography and their applications in neurology, cardiology and oncology. *Phys Med Biol* 2012; **57**: R119–R159. doi: https://doi.org/10.1088/0031-9155/57/21/R119
44. Ter-Pogossian MM, Bergmann SR, Sobel BE. Influence of cardiac and respiratory motion on tomographic reconstructions of the heart: implications for quantitative nuclear cardiology. *J Comput Assist Tomogr* 1982; **6**: 1148–55.
45. Rahmim A, Rousset O, Zaidi H. Strategies for motion tracking and correction in PET. *PET Clin* 2007; **2**: 251–66. doi: https://doi.org/10.1016/j.cpet.2007.08.002
46. W Zhou V, Kyme AZ, Meikle SR, Fulton R. A scheme for PET data normalization in event-based motion correction. *Phys Med Biol* 2009; **54**: 5321–39. doi: https://doi.org/10.1088/0031-9155/54/17/016
47. Conti M. Why is TOF PET reconstruction a more robust method in the presence of inconsistent data? *Phys Med Biol* 2011; **56**: 155–68. doi: https://doi.org/10.1088/0031-9155/56/1/010
48. Mehranian A, Zaidi H. Impact of time-of-flight PET on quantification errors in MR imaging-based attenuation correction. *J Nucl Med* 2015; **56**: 635–41. doi: https://doi.org/10.2967/jnumed.114.148817
49. Angelis GI, Reader AJ, Markiewicz PJ, Kotasidis FA, Lionheart WR, Matthews JC. Acceleration of image-based resolution modelling reconstruction using an expectation maximization nested algorithm. *Phys Med Biol* 2013; **58**: 5061–83. doi: https://doi.org/10.1088/0031-9155/58/15/5061
50. Karakatsanis NA, Tsoumpas C, Zaidi H. Quantitative PET image reconstruction employing nested expectation-maximization deconvolution for motion compensation. *Comput Med Imaging Graph* 2017; **60**: 11–21. doi: https://doi.org/10.1016/j.compmedimag.2016.11.006
51. Qiao F, Pan T, Clark JW, Mawlawi OR. A motion-incorporated reconstruction method for gated PET studies. *Phys Med Biol* 2006; **51**: 3769–83. doi: https://doi.org/10.1088/0031-9155/51/15/012
52. Doot RK, Scheuermann JS, Christian PE, Karp JS, Kinahan PE. Instrumentation factors affecting variance and bias of quantifying tracer uptake with PET/CT. *Med Phys* 2010; **37**: 6035–46. doi: https://doi.org/10.1118/1.3499298
53. Boellaard R. Optimisation and harmonisation: two sides of the same coin? *Eur J Nucl Med Mol Imaging* 2013; **40**: 982–4. doi: https://doi.org/10.1007/s00259-013-2440-9
54. Sunderland JJ, Christian PE. Quantitative PET/CT scanner performance characterization based upon the society of nuclear medicine and molecular imaging clinical trials network oncology clinical simulator phantom. *J Nucl Med* 2015; **56**: 145–52. doi: https://doi.org/10.2967/jnumed.114.148056
55. Carlier T, Ferrer L, Necib H, Bodet-Milin C, Rousseau C, Kraeber-Bodéré F. Clinical NECR in $^{18}$F-FDG PET scans: optimization of injected activity and variable acquisition time. Relationship with SNR. *Phys Med Biol* 2014; **59**: 6417–30. doi: https://doi.org/10.1088/0031-9155/59/21/6417
56. Sorenson JA, Phelps ME, Cherry SR. eds. *Physics in nuclear medicine*. Philadelphia: Elsevier Health Sciences; 2004.
57. Panin VY, Smith AM, Hu J, Kehren F, Casey ME. Continuous bed motion on clinical scanner: design, data correction, and reconstruction. *Phys Med Biol* 2014; **59**: 6153–74. doi: https://doi.org/10.1088/0031-9155/59/20/6153
58. Karakatsanis NA, Garibotto V, Rager O, Zaidi H, IEEE. 2015. Continuous bed motion vs. step-and-shoot acquisition on clinical whole-body dynamic and parametric PET imaging. San Diego, CA, USA: IEEE Nuclear Science Symposium and Medical Imaging Conference.
59. Vanderhoek M, Perlman SB, Jeraj R. Impact of different standardized uptake value measures on PET-based quantification of treatment response. *J Nucl Med* 2013; **54**: 1188–94. doi: https://doi.org/10.2967/jnumed.112.113332
60. Karakatsanis NA, Lodge MA, Zhou Y, Wahl RL, Rahmim A. Dynamic whole-body PET parametric imaging: II. Task-oriented statistical estimation. *Phys Med Biol* 2013; **58**: 7419–45. doi: https://doi.org/10.1088/0031-9155/58/20/7419
61. Zhu W, Li Q, Bai B, Conti PS, Leahy RM. Patlak image estimation from dual time-point list-mode PET data. *IEEE Trans Med Imaging* 2014; **33**: 913–24. doi: https://doi.org/10.1109/TMI.2014.2298868
62. Zanotti-Fregonara P, Chen K, Liow JS, Fujita M, Innis RB. Image-derived input function for brain PET studies: many challenges and few opportunities. *J Cereb Blood Flow Metab* 2011; **31**: 1986–98. doi: https://doi.org/10.1038/jcbfm.2011.107
63. Karakatsanis N, Zhou Y, Lodge M, Casey M, Wahl R, Subramaniam R. Clinical whole-body PET patlak imaging 60-90 min post-injection employing a population-based input function. *J Nucl Med* 2015; **56**(suppl 3): 1786–86.
64. Logan J. Graphical analysis of PET data applied to reversible and irreversible tracers. *Nucl Med Biol* 2000; **27**: 661–70. doi: https://doi.org/10.1016/S0969-8051(00)00137-2
65. Karakatsanis NA, Zhou Y, Lodge MA, Casey ME, Wahl RL, Zaidi H, et al. Generalized whole-body patlak parametric imaging for enhanced quantification in clinical PET. *Phys Med Biol* 2015; **60**: 8643–73. doi: https://doi.org/10.1088/0031-9155/60/22/8643
66. Burger IA, Burger C, Berthold T, Buck A. Simplified quantification of FDG metabolism in tumors using the autoradiographic method is less dependent on the acquisition time than SUV. *Nucl Med Biol* 2011; **38**: 835–41. doi: https://doi.org/10.1016/j.nucmedbio.2011.02.003
67. Watabe H, Ikoma Y, Kimura Y, Naganawa M, Shidahara M. PET kinetic analysis-compartmental model. *Ann Nucl Med* 2006; **20**: 583–8. doi: https://doi.org/10.1007/BF02984655
68. Karakatsanis NA,Lodge MA,Zhou Y,Mhlanga J,Chaudhry MA,Tahari AK,Segars WP,Wahl RL,Rahmim A2011 Dynamic multi-bed FDG PET imaging: feasibility and optimization IEEE Nuclear Science Symposium and Medical Imaging Conference 3863-3870
69. Kotasidis FA, Tsoumpas C, Rahmim A. Advanced kinetic modelling strategies: towards adoption in clinical PET imaging. *Clin Transl Imaging* 2014; **2**: 219–37. doi: https://doi.org/10.1007/s40336-014-0069-8
70. Karakatsanis N,Lodge M,Wahl R,Rahmim A2013 Direct 4D whole-body PET/CT parametric imagereconstruction: concept

and comparison vs. indirect parametric imaging Journal of Nuclear Medicine 54 (suppl 2) 2133
71. Karakatsanis NA, Casey ME, Lodge MA, Rahmim A, Zaidi H. Whole-body direct 4D parametric PET imaging employing nested generalized patlak expectation-maximization reconstruction. *Phys Med Biol* 2016; **61**: 5456–85. doi: https://doi.org/10.1088/0031-9155/61/15/5456
72. Karakatsanis N, Lodge M, Zhou Y, Casey M, Wahl R, Subramaniam R. Novel multi-parametric SUV/patlak FDG-PET whole-body imaging framework for routine application to clinical oncology. *J Nucl Med* 2015; **56**(suppl 3): 625.
73. Karakatsanis N, Lodge M, Fahrni G, Casey M, Zhou Y, Subramaniam R. Simultaneous SUV/patlak-4D whole-body PET: a multi-parametric 4D imaging framework for routine clinical application. *J Nucl Med* 2016; **57**(suppl 2): 367.
74. Carlier T, Bailly C. State-of-the-art and recent advances in quantification for therapeutic follow-up in oncology using PET. *Front Med* 2015; **2**(Article 18): 1–12. doi: https://doi.org/10.3389/fmed.2015.00018
75. Pierce LA, Elston BF, Clunie DA, Nelson D, Kinahan PE. A digital reference object to analyze calculation accuracy of PET standardized uptake value. *Radiology* 2015; **277**: 538–45. doi: https://doi.org/10.1148/radiol.2015141262
76. Zasadny KR, Wahl RL. Standardized uptake values of normal tissues at PET with 2-[fluorine-18]-fluoro-2-deoxy-D-glucose: variations with body weight and a method for correction. *Radiology* 1993; **189**: 847–50. doi: https://doi.org/10.1148/radiology.189.3.8234714
77. Kim CK, Gupta NC, Chandramouli B, Alavi A. Standardized uptake values of FDG: body surface area correction is preferable to body weight correction. *J Nucl Med* 1994; **35**: 164–7.
78. Vanderhoek M, Perlman SB, Jeraj R. Impact of the definition of peak standardized uptake value on quantification of treatment response. *J Nucl Med* 2012; **53**: 4–11. doi: https://doi.org/10.2967/jnumed.111.093443
79. Larson SM, Erdi Y, Akhurst T, Mazumdar M, Macapinlac HA, Finn RD, et al. Tumor treatment response based on visual and quantitative changes in global tumor glycolysis using PET-FDG imaging. The visual response score and the change in total lesion glycolysis. *Clin Positron Imaging* 1999; **2**: 159–71. doi: https://doi.org/10.1016/S1095-0397(99)00016-3
80. Zaidi H, El Naqa I, Naqa E I. PET-guided delineation of radiation therapy treatment volumes: a survey of image segmentation techniques. *Eur J Nucl Med Mol Imaging* 2010; **37**: 2165–87. doi: https://doi.org/10.1007/s00259-010-1423-3
81. Hatt M, Lee JA, Schmidtlein CR, Naqa IE, Caldwell C, De Bernardi E, et al. Classification and evaluation strategies of auto-segmentation approaches for PET: report of AAPM task group No. 211. *Med Phys* 2017; **44**: e1–e42. doi: https://doi.org/10.1002/mp.12124
82. Berthon B, Spezi E, Galavis P, Shepherd T, Apte A, Hatt M. Towards a standard for the evaluation of PET Auto-Segmentation methods: requirements and implementation. *Med Phys* 2017; **44**: 4098–111.
83. O'Connor JP, Aboagye EO, Adams JE, Aerts HJ, Barrington SF, Beer AJ, et al. Imaging biomarker roadmap for cancer studies. *Nat Rev Clin Oncol* 2017; **14**: 169–86. doi: https://doi.org/10.1038/nrclinonc.2016.162
84. Yip SS, Aerts HJ. Applications and limitations of radiomics. *Phys Med Biol* 2016; **61**: R150–R166. doi: https://doi.org/10.1088/0031-9155/61/13/R150
85. Hatt M, Tixier F, Pierce L, Kinahan PE, Le Rest CC, Visvikis D. Characterization of PET/CT images using texture analysis: the past, the present… any future? *Eur J Nucl Med Mol Imaging* 2017; **44**: 151–65. doi: https://doi.org/10.1007/s00259-016-3427-0
86. Orlhac F, Soussan M, Maisonobe JA, Garcia CA, Vanderlinden B, Buvat I. Tumor texture analysis in $^{18}$F-FDG PET: relationships between texture parameters, histogram indices, standardized uptake values, metabolic volumes, and total lesion glycolysis. *J Nucl Med* 2014; **55**: 414–22. doi: https://doi.org/10.2967/jnumed.113.129858
87. Cheng NM, Fang YH, Chang JT, Huang CG, Tsan DL, Ng SH, et al. Textural features of pretreatment $^{18}$F-FDG PET/CT images: prognostic significance in patients with advanced T-stage oropharyngeal squamous cell carcinoma. *J Nucl Med* 2013; **54**: 1703–9. doi: https://doi.org/10.2967/jnumed.112.119289
88. Tixier F, Hatt M, Le Rest CC, Le Pogam A, Corcos L, Visvikis D. Reproducibility of tumor uptake heterogeneity characterization through textural feature analysis in 18F-FDG PET. *J Nucl Med* 2012; **53**: 693–700. doi: https://doi.org/10.2967/jnumed.111.099127
89. El Naqa I, Grigsby P, Apte A, Kidd E, Donnelly E, Khullar D, et al. Exploring feature-based approaches in PET images for predicting cancer treatment outcomes. *Pattern Recognit* 2009; **42**: 1162–71. doi: https://doi.org/10.1016/j.patcog.2008.08.011
90. O'Sullivan F, Wolsztynski E, O'Sullivan J, Richards T, Conrad EU, Eary JF. A statistical modeling approach to the analysis of spatial patterns of FDG-PET uptake in human sarcoma. *IEEE Trans Med Imaging* 2011; **30**: 2059–71. doi: https://doi.org/10.1109/TMI.2011.2160984
91. Hatt M, Majdoub M, Vallières M, Tixier F, Le Rest CC, Groheux D, et al. 18F-FDG PET uptake characterization through texture analysis: investigating the complementary nature of heterogeneity and functional tumor volume in a multi-cancer site patient cohort. *J Nucl Med* 2015; **56**: 38–44. doi: https://doi.org/10.2967/jnumed.114.144055
92. Wang G, Qi J. Direct estimation of kinetic parametric images for dynamic PET. *Theranostics* 2013; **3**: 802–. doi: https://doi.org/10.7150/thno.5130
93. Cheng NM, Fang YH, Yen TC. The promise and limits of PET texture analysis. *Ann Nucl Med* 2013; **27**: 867–9. doi: https://doi.org/10.1007/s12149-013-0759-8
94. Dimitrakopoulou-Strauss A, Strauss LG, Heichel T, Wu H, Burger C, Bernd L, et al. The role of quantitative $^{18}$F-FDG PET studies for the differentiation of malignant and benign bone lesions. *J Nucl Med* 2002; **43**: 510–8.
95. Yan J, Planeta-Wilson B, Carson RE. Direct 4-D PET list mode parametric reconstruction with a novel EM algorithm. *IEEE Trans Med Imaging* 2012; **31**: 2213–23. doi: https://doi.org/10.1109/TMI.2012.2212451
96. Carson R. Tracer kinetic modeling in PET. In: Valk PE, Bailey DL, Townsend DW, Maisey MN, eds. *Positron emission tomography: basic science and clinical practice*. 4th ed. London: Springer-Verlag; 2003. pp. 147–79.
97. Hong I, Cho S, Michel CJ, Casey ME, Schaefferkoetter JD. Complementary frame reconstruction: a low-biased dynamic PET technique for low count density data in projection space. *Phys Med Biol* 2014; **59**: 5441: 5441: 55. doi: https://doi.org/10.1088/0031-9155/59/18/5441
98. Wang G, Qi J. Direct estimation of kinetic parametric images for dynamic PET. *Theranostics* 2013; **3**: 802: 802: 15. doi: https://doi.org/10.7150/thno.5130
99. Reader AJ, Verhaeghe J. 4D image reconstruction for emission tomography. *Phys Med Biol* 2014; **59**: R371–R418. doi: https://doi.org/10.1088/0031-9155/59/22/R371
100. Kotasidis FA, Garibotto V, Zaidi H, IEEE. 2016. Hybrid whole-body dynamic TOF

PET imaging for simultaneous estimation of compartmental and Patlak parametric maps from continuous bed motion data. Strasbourg, France: IEEE Nuclear Science Symposium and Medical Imaging Conference.

101. Cherry SR, Jones T, Karp JS, Qi J, Moses W, Badawi R. Total-body PET: maximizing sensitivity tocreate new opportunities for clinical research and patient care. *J Nucl Med* 2017; jnumed.116.184028: . doi: https://doi.org/10.2967/jnumed.116.184028